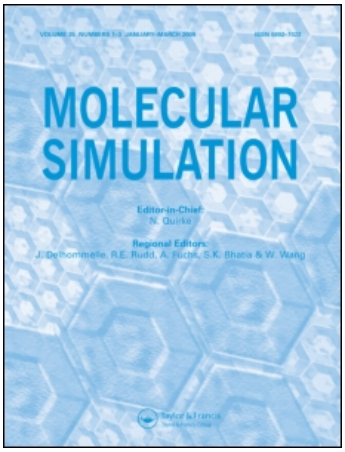

Molecular Simulation

Publication details, including instructions for authors and subscription information:
http://www.informaworld.com/smpp/title~content=t713644482

Modelling oxide thin films

Dean C. Sayle[a]; C. Richard[b]; A. Catlow[b]; Nicu Dulamita[c]; Matthew J. F. Healy[d]; S. Andrada Maicaneanu[ac]; Ben Slater[b]; Graeme W. Watson[e]

[a] Department of Environmental and Ordnance Systems, Royal Military College of Science, Cranfield University, Swindon, UK [b] The Royal Institution of Great Britain, London, UK [c] Technology Department, Faculty of Chemistry and Chemical Engineering, "Babes-Bolyai" University, Cluj-Napoca, Romania [d] Department of Materials and Medical Sciences, Royal Military College of Science, Cranfield University, Swindon, UK [e] Department of Chemistry, Trinity College, Dublin 2, Ireland

Online publication date: 26 October 2010

To cite this Article Sayle, Dean C. , Richard, C. , Catlow, A. , Dulamita, Nicu , Healy, Matthew J. F. , Maicaneanu, S. Andrada , Slater, Ben and Watson, Graeme W.(2002) 'Modelling oxide thin films', Molecular Simulation, 28: 6, 683 — 725
To link to this Article: DOI: 10.1080/08927020290030224
URL: http://dx.doi.org/10.1080/08927020290030224

Molecular Simulation, 2002 VOL. 28 (6-7), pp. 683–725

MODELLING OXIDE THIN FILMS

DEAN C. SAYLE[a,*], C. RICHARD A. CATLOW[b], NICU DULAMITA[c], MATTHEW J.F. HEALY[d], S. ANDRADA MAICANEANU[a,c], BEN SLATER[b] and GRAEME W. WATSON[e]

[a]*Department of Environmental and Ordnance Systems, Cranfield University, Royal Military College of Science, Shrivenham, Swindon SN6 8LA, UK;* [b]*The Royal Institution of Great Britain, 21 Albemarle Street, London W1X 4BS, UK;* [c]*Technology Department, Faculty of Chemistry and Chemical Engineering, "Babes-Bolyai" University, 3400 Cluj-Napoca, Romania;* [d]*Department of Materials and Medical Sciences, Cranfield University, Royal Military College of Science, Shrivenham, Swindon SN6 8LA, UK;* [e]*Department of Chemistry, Trinity College, Dublin 2, Ireland*

(Received April 2001, accepted April 2001)

Three simulation methodologies have been employed to investigate the growth, nucleation, and structure of oxides supported on oxide substrates, these are atom-by-atom deposition, layer-by-layer deposition and finally amorphisation of a structure followed by recrystallisation. The materials which have been investigated include the rocksalt-structured oxides; MgO, CaO, SrO, and BaO, the perovskite structured $SrTiO_3$ and also fluorite structured CeO_2 and ZrO_2. The work has shown that the substrate influences critically the structure of the supported thin film by determining the nature and interactions of defects, dislocations and grain-boundaries, as well as influencing the interfacial ion densities and various epitaxial relationships. In addition, graphical techniques have been employed to show the three-dimensional atomistic structure of each structural and epitaxial feature. Moreover, by considering large simulation cell sizes (approaching the mesoscale, 18 nm square), it has been possible to accommodate the synergistic interactions between neighbouring structural features, which can lead to changes in their basic structure. We also show that the particular surface termination of the substrate can influence the structure (and tentatively, the critical thickness) of the supported film through the example of SrO and TiO_2 terminated faces of a $SrTiO_3$(001) substrate.

Keywords: Oxide; Thin films; Substrate; Amorphisation

*Corresponding author. E-mail: sayle@rmcs.cranfield.ac.uk

ISSN 0892-7022
DOI: 10.1080/08927020290030224

INTRODUCTION

The effect of supporting a thin film on a substrate can have a profound influence upon the properties of the supported material. Indeed, such a phenomenon has been exploited in many applications, which range from catalysis to electronic devices. Moreover, with the advent of new preparative methods and the availability of high-resolution techniques for structural characterisation, the field of surfaces and interfaces has enjoyed explosive growth during the past few years [1,2].

Experimental techniques, such as high-resolution electron microscopy and X-ray diffraction [3,4] have provided valuable structural data on interfaces and grain-boundaries [5–8]. Indeed, such is the resolution of contemporary microscopy techniques that detailed structural models of interfaces at the atomistic level have already been proposed [1,2,9]. For example, Ernst *et al.* have been able to characterise fully the core structure of an edge dislocation within the $SrZrO_3/SrTiO_3$ interface [10]. However, notwithstanding the tremendous advances made, experimental work remains very difficult. Atomistic computer simulation is ideally placed to complement experimental work in this area of interfacial structural characterisation. Indeed, simulation can help to rationalise the detailed atomistic structures and properties of interface systems [11] including growth and nucleation [12,13], supported clusters [14], epitaxy [15–18], buffer layers [12,19], physical and mechanical properties [20–22], dislocations and grain-boundaries [23–34], critical thickness [35] and chemical properties [36,37].

Many theoretical approaches currently used to study structural modifications, in oxides consider "defects" individually and in isolation, moreover, many methodologies pre-define the basic structure of the particular modification, which is then simulated using dynamical and/or static methods. However, such simulations can sometimes result in artificial or unrealistic configurations. For example, since it can be difficult or even intractable to obtain the precise atomistic structure of such configurations experimentally, assumptions (perhaps naïve or indeed incorrect) must be made with regards to the initial structure for the simulation model. Clearly, if the simulated final structure is influenced by the initial "trial" structure, then it may contain artefacts induced by the starting configuration, which may have no relevance to real systems. Consequently, in this field one must devise methodologies for reducing, or preferably, eliminating any influence of the starting structure.

A major challenge one encounters when modelling thin film interfaces is to adequately address the lattice mismatch between the thin film and the underlying support material. For example, the bulk lattice misfit associated with the

SrO/MgO system is approximately +19% based upon inserting the lattice parameters of 5.1 and 4.2 Å for SrO and MgO, respectively, into Eq. (1).

$$\text{Misfit} = \frac{2[n(a_{\text{SrO}}) - m(a_{\text{MgO}})]}{n(a_{\text{SrO}}) + m(a_{\text{MgO}})}, \tag{1}$$

where a_{SrO} and a_{MgO} are the lattice parameters of SrO and MgO, respectively, and n and m are the number of unit cells; for a "bulk" misfit, $n = m = 1$. Assuming that the MgO maintains its natural lattice parameter, then it can be seen, from Eq. (2), that the SrO must be compressed by approximately +18% to facilitate a coherent (on-top) configuration.

$$\text{Compression} = \frac{n(a_{\text{SrO}}) - m(a_{\text{MgO}})}{n(a_{\text{SrO}})} \tag{2}$$

(Eqs. (1) and (2) refer to rocksalt-structured materials and assume the same orientation of the lattices at the interface. For the general case, we refer the interested reader to Ref. [38]).

Clearly, straining the SrO to accommodate a 17.6% reduction in lattice parameter requires considerable energy and it is unlikely that such a configuration will actually exist. Alternatively, one can explore various epitaxial relationships between the SrO and MgO with lower associated lattice misfits. For example, four SrO unit cells overlying five MgO unit cells has an interfacial lattice misfit of only −2.9% (Eq. (1); $n = 4$, $m = 5$). Here the SrO must be expanded to bring the two lattices into commensuration. One can employ a Near Coincidence Site Lattice theory (NCSL) to generate configurations with low associated lattice misfits [38]. Indeed, atomistic simulation methodologies are ideally suited to explore such configurations [18] albeit that one must consider systematically a wide range of configurations to generate reliable statistics. In addition, although it is possible to generate an interface system based upon some NCSL, it is likely that there will be problems in matching the lattice locally. Moreover, for real systems one must include additional structural complexities such as defects, dislocations, grain-boundaries, and reduced interfacial ion densities, which all contribute to reduce the lattice misfit. Clearly, such structural modifications can have a profound influence on the material properties. Some structural modifications may prove beneficial and can be exploited; for example within catalytic systems [36,39], whilst others may be deleterious, such as dislocations within high T_c superconductors that one must endeavour to eliminate from the material [40].

To generate realistic models of supported oxide thin film, the models must include all the important structural modifications such as epitaxial relationships, defects and reduced interfacial ion densities. The defects (which often evolve to

reduce lattice misfit) may include grain-boundaries, dislocation arrays, vacancies, substitutionals, interstitials and clusters of such defects. Moreover, such modifications can evolve within both the supported thin film and the underlying substrate. The inclusion of all these structural features is clearly a challenging undertaking, but nevertheless must be achieved to generate a realistic model. Many simulations are based upon constructing a trial system, which includes all the required structural features and then applying energy minimisation or dynamical methods to the system. However, as discussed previously, this approach is no longer appropriate for these problems since the epitaxial relationships, the nature, location and concentration of defects, dislocations arrays and grain-boundaries present a prohibitively high number of permutations. In addition, the inclusion of a dislocation will influence the structure of neighbouring dislocations. Essentially, the synergistic interaction between each component structural feature and the structural influence of such interactions must also be included within the model.

A second important consideration when generating models for thin films is that the mode of preparation can influence the final structure [2], or more optimistically, one might suggest that the structure can be controlled by manipulating the preparative conditions. Essentially, the particular growth and nucleation mechanisms can exact a significant influence on the structure of the supported thin film and considerable efforts have been focussed on addressing these issues [1]. Accordingly, atomistic computer simulation methodologies for modelling thin film interfaces must include all the structural features observed within real systems (including their interactions) and reflect also the particular experimental method by which the films were prepared. The latter may be achieved, in part, by introducing growth and nucleation mechanisms within the simulation methodology.

In this study, we focus on including various structural features and their interactions, by introducing simple growth and nucleation mechanisms within our simulations. We start by exploring oxide–oxide systems with the rocksalt type structure, specifically, CaO/MgO(001) and SrO/BaO(001) fabricated using an atom-deposition methodology. The MgO/CaO(001) system is then considered using a layer-by-layer approach. To accommodate larger simulation cells we use the amorphisation and recrystallisation methodology and apply it to the SrO/MgO(001) and MgO/BaO(001) systems. We next investigate whether the structure of the substrate influences the structure of the thin film on which it is supported. Specifically, we consider MgO supported on $SrTiO_3$(001), which, in addition, offers two surface terminations, a SrO terminated or TiO_2 terminated (001) surface. Finally, we consider CeO_2/ZrO_2(111) in order to determine whether the amorphisation and recrystallisation methodology is a sufficiently

robust tool (given the available potential models) to use in the exploration of supported fluorite structured oxides.

METHODOLOGY

Two simulation codes, MARVIN [41] and DL_POLY,* were used to perform the energy minimisation and dynamical simulations reported in this study. The MARVIN code (energy minimisation and dynamical simulation) was used for the "atom deposition" and "layer-by-layer" methodologies, whilst DL_POLY (dynamical simulation) was used to perform the "amorphisation and recrystallisation".

The MARVIN code, which employs two-dimensional periodic boundary conditions, considers the crystal as a stack of ions periodic in two-dimensions, where the stack consists of a whole number of repeating units in the direction normal to the interface. The stack is subdivided into two regions: a region I, where all the ions are allowed to relax explicitly, and a region II, where the ions are all held fixed relative to each other. Region II is included to ensure that the long-range effects of the ions in the bulk of the crystal on the surface region are represented correctly. The top of region I is the free surface, onto which ions comprising the thin film are deposited thus creating the interface.

In contrast, DL_POLY performs atomistic dynamical simulations using three-dimensional periodic boundary conditions and therefore the surface is simulated using a periodic array of slabs with a void introduced, perpendicular to the interfacial plane, to represent the vacuum above the surface of the thin film. The void is, of course, sufficiently large to ensure that the interactions between slabs are negligible. In accordance with the procedure described above for the MARVIN code, a standard two-region methodology was employed with DL_POLY.

The reason for using the DL_POLY code for the amorphisation and recrystallisation, is that it is considerably faster for the simulations presented here. In particular, the smallest vector is introduced perpendicular to the surface to generate the vacuum above the thin film, which facilitates a very efficient three-dimensional summation. Many simulations of surfaces performed using three-dimensional codes are inefficient due to the large sampling of reciprocal lattice vectors perpendicular to the surface in the Ewald sum compared with the

*DL_POLY is a package of molecular simulation routines written by W. Smith, T.R. Forester, copyright The Council for the Central Laboratory of the Research Councils, Daresbury Laboratory, Daresbury, Warrington, U.K. (1996).

other two directions. In addition, by performing dynamical simulations on a parallel computer (typically the calculations require 10 days using 16 processors of a Silicon Graphics Origin 2000) we also benefit from the efficiency of the DL_POLY code when run in parallel.

The reliability and quality of the simulation is critically dependent upon the potential models describing the materials under investigation. The interionic potentials used in this present study are, as is normally the case for metal-oxides, based on the Born model of the ionic solid in which the ions interact via long-range Coulombic interactions and short-range, parameterised interactions. Potential parameters for the rocksalt and perovskite structured oxides considered in this study were taken from Lewis and Catlow [42], whilst those for CeO_2 and ZrO_2 from Lewis and Catlow and Dwivedi and Cormak [42,43]. In addition, for all the systems considered, a rigid ion model was imposed to reduce the computational expense.

For the supported thin films, we define a thin film (TF) interface energy as:

$$\gamma_{\mathrm{TF\,interface}} = (E_{\mathrm{TF\,interface}} - E_{\mathrm{bulk}} - n(E_{\mathrm{TF}}))/\mathrm{Area}, \tag{3}$$

where $E_{\mathrm{TF\,interface}}$ is the total energy of the interface, E_{bulk} the bulk energy of the substrate, E_{TF} the standard three-dimensional periodic bulk energy for the supported thin film material per formulation unit and n is the number of formula units of the supported thin film.

Three simulation methodologies, represented graphically in Fig. 1, have been developed to explore the growth nucleation and structure for supported thin film systems, which we designate: "atom deposition", "layer-by-layer" and "amorphisation and recrystallisation".

Atom Deposition

The interface is generated by successively depositing individual ions onto the substrate until the required thickness of the supported film is achieved. A small driver program was written to automate this deposition process and was used in conjunction with the MARVIN code, which performed the minimisation and dynamical simulations. The code introduces the ions, comprising the thin film, at random positions above the substrate surface, within the bounds of the vectors describing the surface of our simulation cell, and moves them vertically towards the surface until they are within 2.5 Å of the surface or any previously deposited species. Energy minimisation and/or dynamical simulation are then applied to the system (comprising the species deposited and the support material) after which, additional species are added and the cycle repeated until the required thin film thickness is reached. Since dynamical simulation is applied to the system after

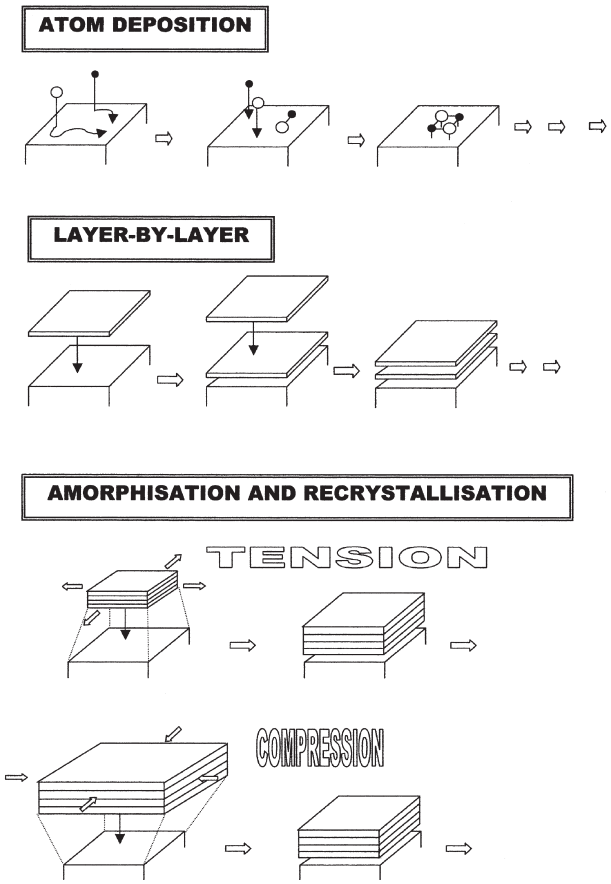

FIGURE 1 Schematics illustrating the three methodologies employed in this study.

each deposition step, the approach is computationally expensive and therefore the use of large simulation cell sizes and/or deposition levels may not be possible. Conversely, the merits of this approach include the investigation of epitaxial growth mechanisms, nucleation sites and the generation of clusters at sub-monolayer deposition levels.

Layer-by-layer

Here, the interface is fabricated via the sequential deposition of monolayers onto the substrate surface. In particular, the methodology commences with the construction of the first complete monolayer on the substrate surface before the

layer and interface region are subjected to dynamical simulation and energy minimisation. Each successive monolayer is similarly "deposited" (and dynamical simulation and energy minimisation are imposed) until the desired film thickness is reached. Because the dynamical simulation is applied only after the addition of each monolayer as opposed to each atom, the procedure is less computationally expensive and larger cells may be addressed.

Amorphisation and Recrystallisation

This technique involves constraining the supported thin film under either high compression or tension. The subsequent application of high temperature dynamical simulation to the system results in the thin film undergoing an amorphous transition as the system relaxes. Prolonged dynamical simulation is then required to allow the system to recrystallise under the influence of the support. As the thin film recrystallises, structural modifications evolve naturally as the system accommodates the lattice misfit. In addition, the synergy of interactions between the various structural features (between dislocations, for example) will be implicit within the simulation and each "defect" will evolve structurally in response to such synergistic interactions.

The recrystallisation process is considered to be complete when the system is no longer evolving structurally or energetically; the duration of which depends on the particular system. Central to this methodology is the fact that dynamical simulation as applied to an amorphous structure, allows a more comprehensive exploration of the configurational space compared with a crystalline material owing to the high energy starting point of the amorphous structure and the conformational freedom that arises from this. In particular, the initial strain (tensile or compressive) under which the thin film is constrained is critical in generating the desired high-energy amorphous transition. If the strain is too low, the system may not amorphise and the system will not evolve any structural modifications since the energies required to surmount the energy barriers and introduce such defects within a crystalline material are higher than that can be explored within the timescales accessible using dynamical simulations. Even for strains sufficient to create amorphisation, it is possible that the strain energy is still insufficient to prevent the evolving structure from becoming trapped in local energy minima during the short time periods that can be simulated with finite computing power. To avoid this problem and maximise the utility of the amorphisation and recrystallisation methodology, the strain must be sufficiently high that the ions have enough energy to explore adequately the potential hypersurface and settle at low energy sites. Conversely, if the initial amorphous

inducing strain is too high, the velocities of ions will be so high that the thin film will loose all integrity and the simulation will fail catastrophically. Preliminary calculations suggest that the appropriate initial strain is system dependent; for simple binary oxides the tolerances are high and a wide range of strains are valid, whilst we found the tolerances to be narrow for systems with the fluorite structure.

Whilst the initial strain imposed upon the supported thin film dominates the amorphisation process, the temperature at which the dynamical simulation is performed plays an additional, but important role. For example, the amorphisation is as efficient at 20 K as at 2000 K, but the recrystallisation process at 20 K is much slower, reflecting the reduced mobility at this temperature. In essence, the optimum temperature is one that allows the structure to evolve but falls short of melting the thin film, which would be detrimental as it would prevent recrystallisation and require an additional quenching step [44].

An additional important feature of the methodology is that the amorphous transition enables all memory of the initial prepared configuration to be lost, which, as argued earlier is particularly important in these systems.

It is tempting to suggest that the simulated recrystallisation models real recrystallisation processes. However, the amorphous starting configurations are of high energy and do not therefore reflect real systems. Moreover, temperature scaling must be performed during the simulation to prevent the rapid build up of large amounts of excess kinetic energy as the system evolves from the highly strained initial configuration, via an amorphous transition, to a crystalline phase with defects and reduced strain. In addition, the timescales required to effect the recrystallisation are much smaller compared with real crystallisation. Typically, they are of the order of a nanosecond. The simulation is therefore a technique to derive a range of low energy configurations, which comprise various structural features observed in real systems and the evolution or dynamical recrystallisation bears little physical significance.

In contrast to the atom-deposition or layer-by-layer methodology, this amorphisation and recrystallisation methodology is relatively inexpensive computationally and much larger simulation cells may be considered. Accordingly, large defects may be considered, such as dislocation networks that exist at the mesoscale. Conversely, information regarding nucleation and growth mechanisms and indeed the ways in which such growth influences the resulting structure is limited.

Clearly, all three methodologies are complementary and when used in parallel will provide information spanning the structure of thin films, the influence of growth, nucleation mechanisms, and structural changes that might arise as a consequence of the nature (structure) of the substrate material. Moreover,

simulation may be applied to explore large structural features (approaching the mesoscale) such as dislocation networks.

We now apply the three methodologies to various systems. We start with small simulation cells and explore nucleation and growth and their influence on thin film structures and then extend our study to include larger systems using the amorphisation and recrystallisation methodology.

ATOM DEPOSITION

We first consider the CaO/MgO(001) system, which has an associated lattice misfit of $+13\%$.

CaO/MgO(001)

Thin CaO films were generated on an MgO(001) substrate 635 Å^2 in size using the atom deposition methodology described above. Further details regarding the simulation procedure can be found in Ref. [19].

After the deposition of 1.5 equivalent monolayers (Fig. 2(a)), the interface consists predominantly of areas where the layer is still one monolayer thick and the CaO exposes the (100) orientation to the substrate, whilst at the ridges (where the layer is thicker) the orientation is CaO(110). In both regions, the Ca and O ions still lie directly above their respective O and Mg counter ions of the support. Upon further deposition (1.8 equivalent monolayers), the CaO can be seen to expose both (310) and (100) surfaces at the interface (Fig. 2(b)); a schematic to aid interpretation of this structure is included within this figure. Since the CaO(310)/MgO(100) interface is associated with a -10% misfit, this region compensates for the $+13\%$ misfit associated with the adjoining CaO(100) region. Specifically, the lattice misfit is reduced further by areas of CaO under tensile stress balanced by adjoining CaO regions constrained under compressive strain. Close inspection of Fig. 2(b) reveals a degree of rumpling on the surface of the CaO thin film, which facilitates a further reduction in the lattice misfit and improves the registry between counter-ions across the interface.

It is perhaps surprising to observe such high values for the misfit (i.e. -10 and $+13\%$). However, since the film thickness is less than three layers, the strain energy terms are outweighed by the favourable interfacial interactions. Conversely, for thicker films a configuration with this misfit cannot be sustained, since in contrast to the interfacial interactions the strain energy terms are additive for each additional layer and at some particular "critical" thickness [35],

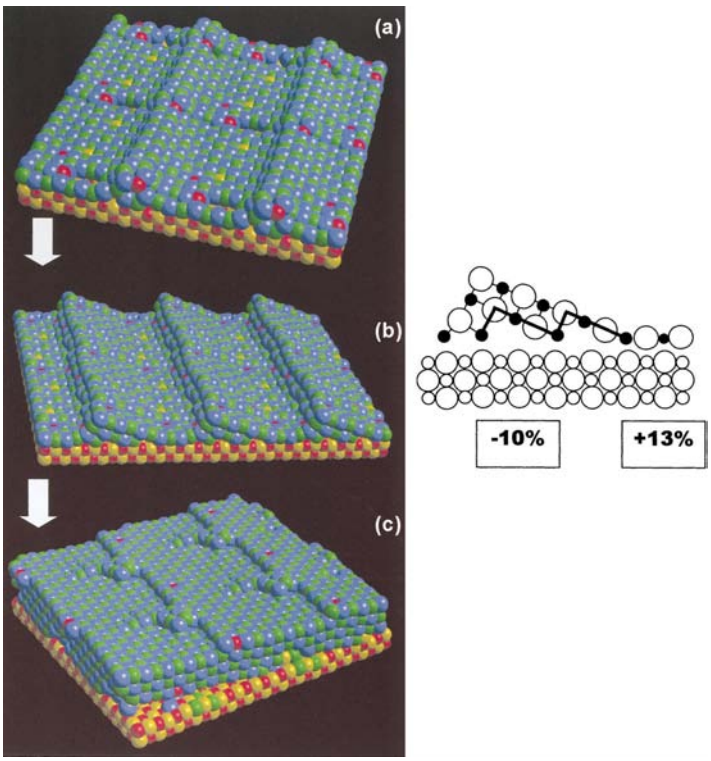

FIGURE 2 Representation of the CaO/MgO(100) system after the deposition of (a) 1.5, (b) 1.8 and (c) 3.6 equivalent CaO monolayers onto the MgO surface. A schematic for (b) is included to aid interpretation of the figure. Calcium is coloured blue, magnesium is yellow, oxygen (CaO) is green and oxygen (MgO) is red. For reasons of clarity only two layers of the MgO(001) surface is depicted.

structural changes will occur. Accordingly, after the deposition of 3.6 equivalent monolayers, the CaO thin film is observed to have rotated by about 5° with respect to the underlying MgO support (Fig. 2(c)) while exposing only the (100) surface at the interface. By assigning this configuration to a particular NCSL [38], we can estimate that the configuration is associated (geometrically) with a lattice misfit of $+5\%$. In addition, dislocations have formed within the CaO, which are indicated by the monatomic steps and kinks present on the surface. Since kink sites exhibit low coordinative saturation, they may act as nucleation centres. Indeed, careful inspection of Fig. 2(c) reveals growth at these regions, indicated by the presence of small CaO clusters. The presence of such dislocations in conjunction with lattice relaxation will reduce further the 5% misfit associated with this configuration.

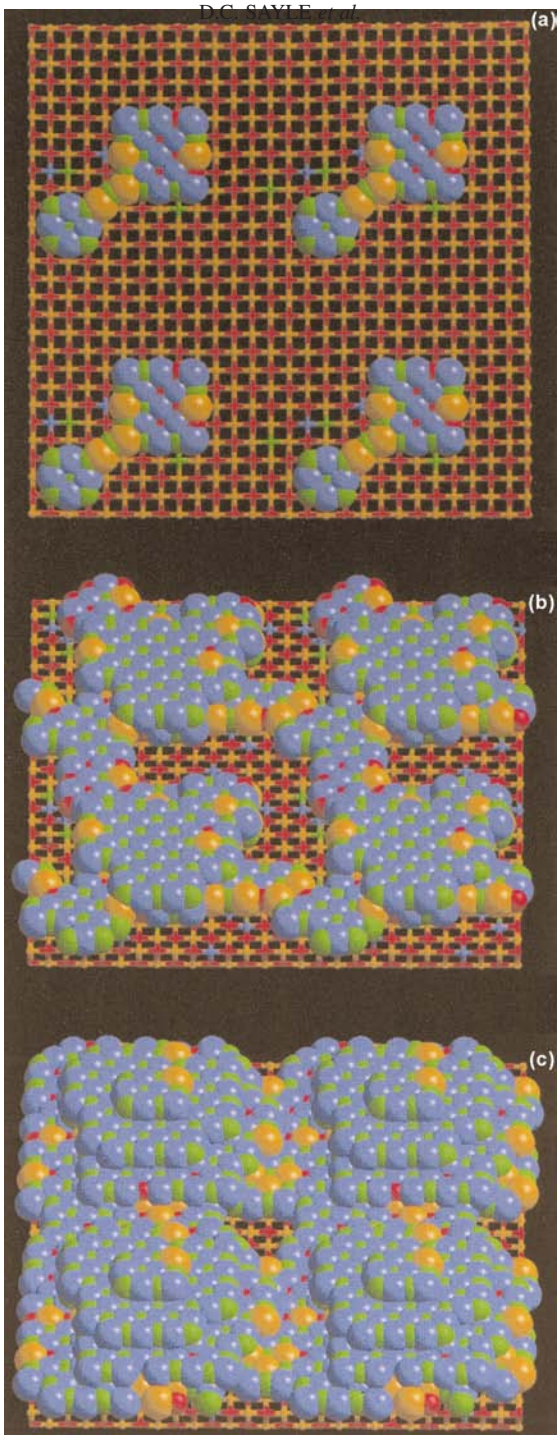

Inevitably, the small size of the simulation cell size considered in this section will preclude the evolution of certain structural features. For example, one might speculate that a configuration with 100 CaO units lattice matched with 114 MgO units for the underlying support (+0.3% misfit) might be stable. However, to test such a configuration a simulation cell of 100×100 MgO units in size would be required. However, the simulation does provide useful insights into the structural modifications that the overlying thin film may accommodate to reduce the misfit, such as the exposure of different CaO surfaces and the formation of dislocations and lattice rotations. Clearly, the availability of increased computational resources will enable the identification of additional structural features leading to a greater understanding of epitaxial processes.

We now apply the atom deposition methodology to a system in which there is a negative associated lattice misfit.

SrO/BaO(001)

The lattice parameters for SrO and BaO are 5.16 and 5.54 Å, respectively, and therefore this system is associated with a lattice misfit of −6.8%. Following the atom deposition methodology, SrO species were deposited on a 1094 $Å^2$ BaO(001) substrate. At sub-monolayer deposition levels, the SrO was observed to form small clusters on the BaO surface (Fig. 3(a)). We also notice that Ba and O species migrate from the surface of the underlying BaO support to occupy Sr and O lattice positions within the SrO clusters and the displaced Sr and O species then fill the vacant sites on the BaO surface, resulting in lattice mixing. At about one monolayer (equivalent) coverage, the surface of the BaO is not completely covered; rather a second SrO layer forms on top of the first (Fig. 3(b)). Finally, after about two (equivalent) monolayers have been deposited, a third SrO layers becomes populated (Fig. 3(c)) resulting in the formation of a square pyramidal SrO cluster. We also notice Ba atoms accommodating Sr lattice positions within the SrO cluster extending as far as the third SrO layer at the top of the cluster. Further details of this system are described by Sayle *et al.* [45]

We next consider the MgO/CaO(001) system constructed via a layer-by-layer methodology [45].

FIGURE 3 Representation of the SrO/BaO(100) system; (a) submonolayer coverage; (b) equivalent monolayer coverage; (c) two equivalent monolayers. Barium is coloured orange, oxygen (BaO) is red, strontium is blue and oxygen (SrO) is green.

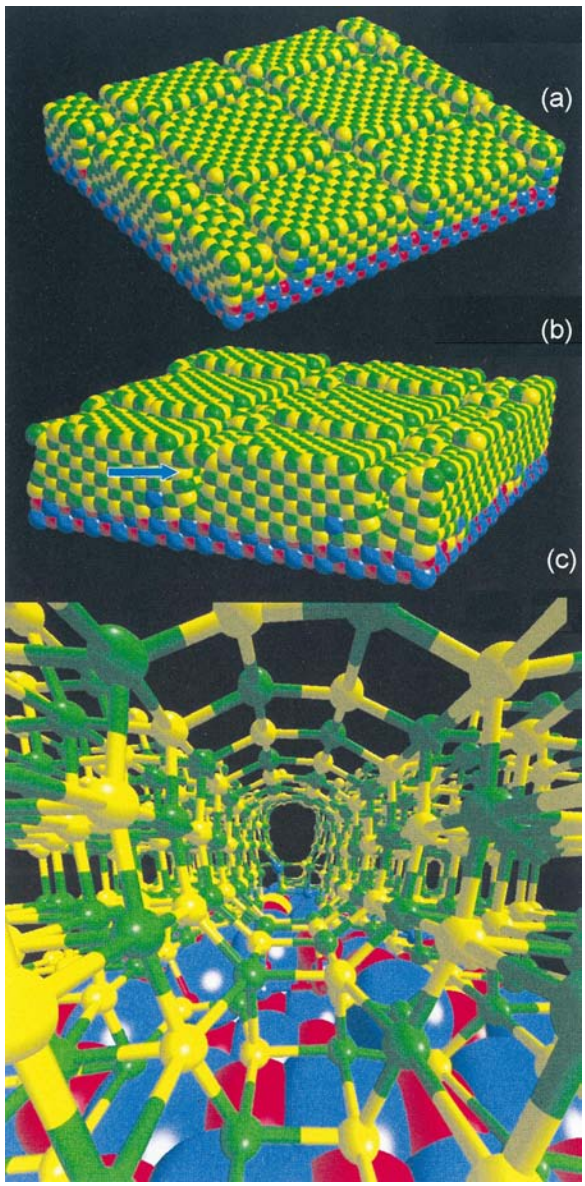

FIGURE 4 Structure of the MgO/CaO(001) system after the deposition of (a) four MgO layers; (b) six MgO layers; (c) perspective view along the direction of the arrow depicted in Fig. 4(b). Magnesium is coloured yellow, calcium is blue, oxygen (MgO) is green and oxygen (CaO) is red.

LAYER-BY-LAYER

MgO/CaO(001)

The MgO/CaO(001) system, which is associated with a −13% lattice misfit, was generated within a 828 Å^2 simulation cell size by successively depositing MgO(001) monolayers (one atom thick) directly on top of a CaO(001) substrate following the "layer-by-layer" procedure described above.

After three to four MgO layers are deposited, the MgO thin film starts to display small "cracks" or grooves (Fig.4(a)). Initially, the MgO is coherent with respect to the underlying CaO(001) and therefore accommodates the full (bulk) lattice misfit, and is therefore under tension. Subsequently, to reduce the tensile stress within the MgO, the lattice contracts to its natural lattice parameter resulting in cracks within the MgO, thin film. Radial distribution functions (RDF) were calculated for each of the MgO layers and revealed that the average Mg–O bond distances in consecutive planes from the top surface down were 2.05, 2.10, 2.17, and 2.25 Å compared to 2.35 Å for the Ca–O interfacial plane. The Mg–O and Ca–O bond distances in the parent oxides are 2.1 and 2.4 Å, respectively. After the deposition of six layers (Fig. 4(b)), the "cracks" appear to be capped, which may indicate the start of an edge dislocation. The Burgers vector for the dislocation would be parallel to the surface, which implies that the density of the layer increases with the introduction of the dislocation. In addition, to maintain charge continuity, the "cap" comprises both Mg and O ions. The resulting thin film structure therefore accommodates surprisingly large channels of approximately 5 Å diameter, which propagate through the full length of the MgO film as simulated within this cell size. An enlarged, perspective view, looking down one of the channels, is presented in Fig. 4(c). The driving force for such behaviour is again a reduction in the strain energy of the system. For example at the interface, the MgO lies coherent with the CaO support accommodating the full −13% lattice misfit; the stability generated from the perfect alignment of cations and anions across the interface outweighs the strain energy of the MgO lattice. Conversely, further from the lattice the MgO relaxes back to its natural lattice parameter at which point there is sufficient space to include an additional "line" (edge dislocation) of MgO units. We suggest therefore that Fig. 4(c) is a view looking down this dislocation core. The lattice misfit can be estimated to be approximately +2% based upon 14 MgO lattice planes lattice matched with 12 CaO lattice planes (Fig. 4(b)).

The interface energy for deposited film thicknesses from 1 to 6 monolayers is presented in Fig. 5 and demonstrates an almost linear relationship, which is consistent with strain energy terms being cumulative. Between 3 and 4 layers, the

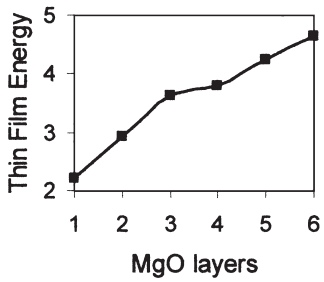

FIGURE 5 Calculated thin film energies as a function of thickness for 1–6 MgO layers deposited.

energy appears to reach a plateau as the dislocation is introduced into the system (critical thickness). However, as further MgO planes are deposited, the energy increases again linearly as the dislocation only relieves partially the strain within the system. Note also the small reduction in gradient from 4–6 layers compared with 1–3 layers, which is attributed to the reduced strain within the MgO planes as a consequence of the dislocation. Nevertheless, the strain energy contribution for each additional MgO layers cannot be sustained and therefore other structural modifications will be introduced within the system if the deposition continues.

Although atom-deposition and layer-by-layer methodologies generate useful information regarding the structure, growth and nucleation of thin films they are limited by the size of the simulation cell considered. Accordingly, to incorporate more structural information within the model (such as dislocation networks and grain-boundaries that have been observed within real systems) the simulation cell size must be increased. In the following sections, we consider simulation cells that are two orders of magnitude larger than have been considered so far and employ a simulated amorphisation and recrystallisation methodology.

AMORPHISATION AND RECRYSTALLISATION

We first consider the SrO/MgO(001) system, which is associated with a +19% lattice misfit.

SrO/MgO(001)

To explore the structural features associated with a SrO thin film, when supported on an MgO(001) substrate, the amorphisation and recrystallisation methodology was employed. A thin film of SrO was placed on top of an MgO(001) substrate and the SrO was then constrained under considerable pressure to induce the

amorphisation. Three simulation cell sizes were employed to explore the influence of the cell size on the final structures. Specifically, cell sizes of approximately 3500, 13,800 and 31,100 $Å^2$ were considered. All three cells were simulated with the DL_POLY code, but the smallest cell was also simulated with the MARVIN code to ensure that two- and three-dimensional periodic boundary condition strategies deliver analogous structural models. The models generated by the two codes exhibited no appreciable differences with respect to relative stabilities (thin film energies) and structural features indicating that the application of three-dimensional periodic boundary conditions with a void to represent the free surface was a valid approach. Further details of the simulation can be found elsewhere [27,45].

To monitor the amorphisation and subsequent recrystallisation, RDF and mean square displacements (MSD) of the ions were calculated during the dynamical simulations. For the purpose of illustration, the simulation using a cell size of 13,800 $Å^2$ will be considered in the following paragraphs, although we note that all three simulations exhibit comparable structural features.

Analysis of the Amorphous Phase

The MSD of strontium during the high temperature dynamical simulation phase is shown in Fig. 6. It increases rapidly at the start of the simulation, but reaches a plateau as the rate of diffusion decreases. The increase in the MSD at the start of the simulation represents the large displacements induced by relaxation of the high initial strain and indicates the initial amorphisation. However, after 100 ps the MSD levels off indicating that there is little diffusion once the recrystallisation has occurred.

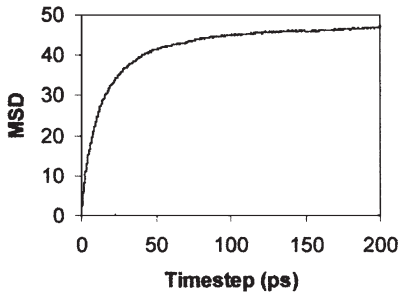

FIGURE 6 Calculated strontium MSD within the SrO/MgO(001) system during dynamical simulation performed at 2200 K. The units for the MSD are $Å^2$.

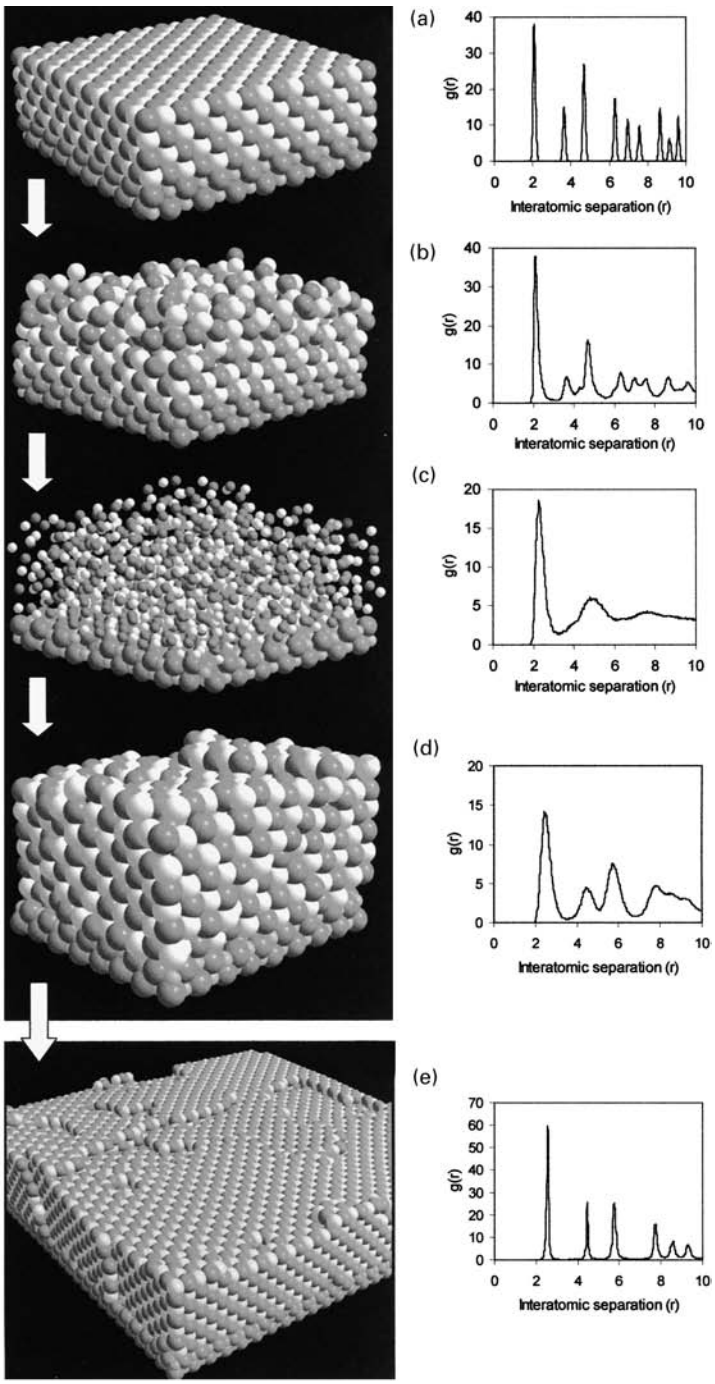

Figure 7(a)–(d) shows a small segment of the simulation cell (8%) during the amorphisation and recrystallisation, where Fig. 7(a) depicts the starting structure. To the right of each figure the RDF relating to each particular structure is presented. Initially, the regular structure of the surface of the SrO thin film starts to break up (Fig. 7(b)) and is associated with an expansion of the thin film along the surface normal as the SrO endeavours to eliminate the strain associated with the initial compression of the SrO lattice. As the dynamical simulation progresses, the break up of the thin film extends further from the surface towards the interfacial plane. Finally, after 0.75 ps the SrO thin film becomes amorphous (Fig. 7(c)). Under prolonged dynamical simulation, the SrO starts to recrystallise back into the rocksalt structure (Fig. 7(d)) and the final structure at the end of the simulation is shown in Fig. 7(e) which depicts a larger segment of the full simulation cell compared with Fig. 7(a)–(d). Inspection of the RDF for each structure reveals that the sharp peaks of the starting structure (Fig. 7(a)) broaden (Fig. 7(b)) and eventually lose all long-range order whilst retaining some short-range order (Fig. 7(c)). We suggest, therefore, that the SrO undergoes an amorphous transition, but does not liquefy. After prolonged dynamical simulation (25 ps, Fig. 7(d)), the SrO appears to regain some long-range order, essentially the SrO is starting to recrystallise from the *amorphous solid*. At the end of the simulation, the final structure can be seen to be highly crystalline as indicated by the sharp peaks within the RDF (Fig. 7(e)).

Structural Features

The final SrO/MgO(001) thin film structure, shown in Fig. 7(e), comprises between six and seven layers of SrO supported on MgO (that the SrO undergoes an amorphous transition, negates any significance attributable to the starting number of layers). The nearest neighbour distances for Sr–O were calculated to be 2.57 ± 0.1 Å, which is consistent with natural SrO and indicates very little strain with the SrO lattice. Chern [46] who fabricated MgO, SrO and NiO thin films supported on MgO(001) and $SrTiO_3$(001) observed that the lattice parameters of the thin films were slightly compressed in first few layers (2% for the first monolayer) but relax back to the bulk lattice parameters further from the interface.

FIGURE 7 Sphere model representations of a segment of the SrO/MgO(001) system during the simulated amorphisation and recrystallisation; (a) starting structure; (b) after 0.25 ps; (c) 0.75 ps; (d) 25 ps and (e) final structure. The latter depicts the full simulation cell. To the right of each figure the corresponding Sr–O RDF is presented (values for the abscissa measured in Å).

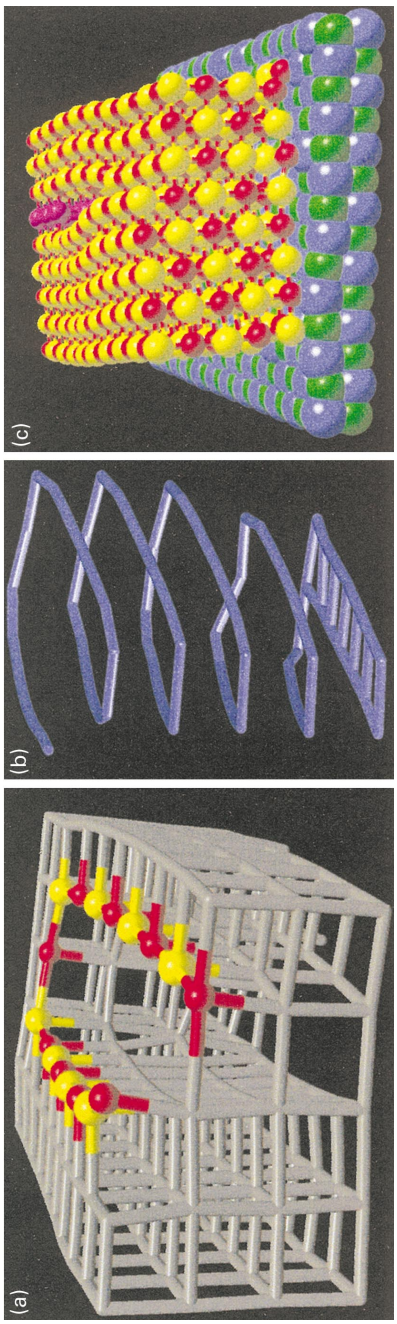

FIGURE 8 Structure of a typical screw-edge dislocation within the supported SrO thin film; (a) representation of part of the SrO lattice (coloured grey) surrounding the dislocation; (b) stick representation of the spiral of Sr and O atoms; (c) ball and stick representation showing more clearly the edge component (coloured purple) of the dislocation. Strontium is yellow, magnesium is blue, oxygen (SrO) is red and oxygen (MgO) is green.

Defects

Intermixing of cations across the interface occurs: For the interfacial MgO layer, 3% of the magnesium lattice sites become occupied by strontium ions while the displaced magnesium ions are incorporated into strontium lattice positions within the two SrO planes closest to the interface. Such behaviour is similar to that observed in a study by Lind *et al.* on the Fe_2O_3/NiO system [47] in which inter-diffusion between the Fe_2O_3 and NiO was observed to be of the order of 1 or 2 atomic layers. The interfacial SrO layer has a much lower density of ions (70% occupancy) compared with SrO layers further from the interfacial plane. In particular, there are many voids with sizes ranging from 2 to 10 nm^2. Tasker and Stoneham have suggested that a reduced density of ions at the interface enhances interfacial stability [16]. We also observe a large rumpling of ions within the MgO interfacial layer; Mg–O distances normal to the interface range from 1.9 to 2.8 Å. Such behaviour occurs to increase the number of energetically favourable cation–anion interactions across the SrO and MgO interfacial plane and thereby stabilise the system by increasing the interfacial adhesion.

Dislocations

Figure 8(a) depicts the structure of a dislocation observed within the SrO thin film, with Fig. 8(b) showing the core structure. The dislocation, which traverses the entire thickness of the thin film, clearly has mixed screw-edge character (Fig. 8(c)) and is typical of many that were observed within the system comprising the complex dislocation network.

Figure 9(a) shows a slice cut parallel to the interfacial plane through the SrO; only 17 of the 138 nm^2 is shown to maintain the clarity of the figure. The figure depicts a particular SrO domain, rotated by about 6° relative to the surrounding SrO crystal, which is facilitated by four edge dislocations traversing the entire thickness of the thin film. Inspection of the dislocations reveals that the Burgers vectors lie at 45° to the line of the dislocations indicating they have both screw and edge character (Fig. 9(b)). Figure 9(c) shows segments of each of the four screw-edge dislocations depicting their relative positions within the SrO thin film.

Epitaxial Relationships

Characterisation of the commensurate relationships that exist between the SrO and underlying MgO cannot be defined precisely as the structures have high dislocation densities and include many domains rotated about low angles.

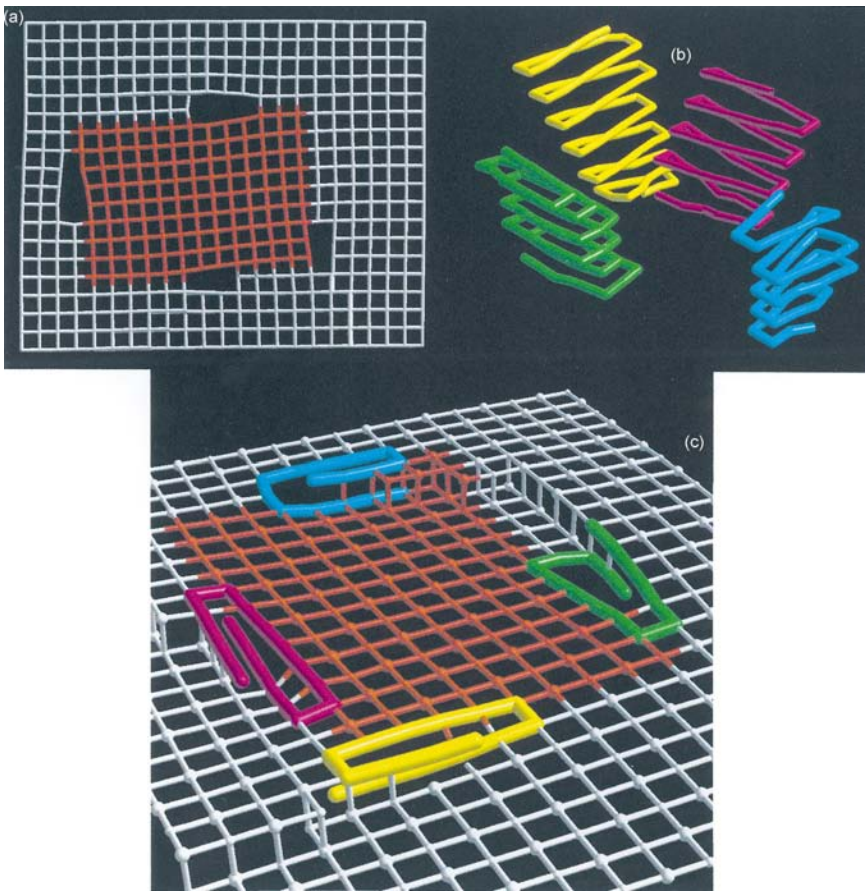

FIGURE 9 Graphical representation of a subdomain within the supported SrO crystal, which has rotated by about 6° facilitated by four screw-edge dislocations; (a) stick representation of a slice cut parallel to the interfacial plane through the SrO thin film, depicting the rotated SrO subdomain (red) within part of the surrounding SrO lattice (white); (b) stick representation of the core structures for each of the four dislocations; (c) superposition of the dislocation core structures and rotated SrO subdomain. Only part of the dislocation cores are shown in (c) for reasons of clarity.

Moreover, the detailed relaxation of the ions acts to compound this difficulty. However, one can loosely characterise geometrically the majority of the domains within the SrO with respect to the underlying MgO(001) as conforming to eight SrO(020) interplanar spacings (2.57 Å) lattice matched with 10 MgO(020) (2.1 Å), which is associated with a lattice misfit of -2.3%. Clearly, other regions within the SrO thin film (for example the rotated domains) will accommodate slightly different epitaxial configurations with respect to the underlying MgO support.

In the following section, we apply the amorphisation and recrystallisation methodology to a system where the bulk lattice misfit is highly negative. Specifically we consider the MgO/BaO system, which has an associated (bulk) lattice misfit of -27%. In addition, to induce amorphisation, the MgO was constrained under tensile stress in contrast to the compressive strain employed to induce amorphisation for the previous SrO/MgO(001) system.

MgO/BaO(001)

The application of dynamical simulation to the MgO/BaO(001) system, with the MgO thin film constrained initially under tension again resulted in the amorphisation of the MgO thin film, which under prolonged dynamical simulation recrystallised revealing a wealth of structural features. The calculated RDF for the amorphous thin film (after 1 ps of dynamical simulation) is presented in Fig. 10(a), which shows broad peaks reflecting the amorphous nature of the thin film, whilst the RDF for the final structure is shown in Fig. 10(b). Further details of the simulation can be found elsewhere [28].

The structure of the MgO/BaO(001) system is presented in Fig. 11, where for the purpose of clarity only one quarter of the full simulation cell is shown. However, the segment is sufficient to demonstrate the complexity of the system.

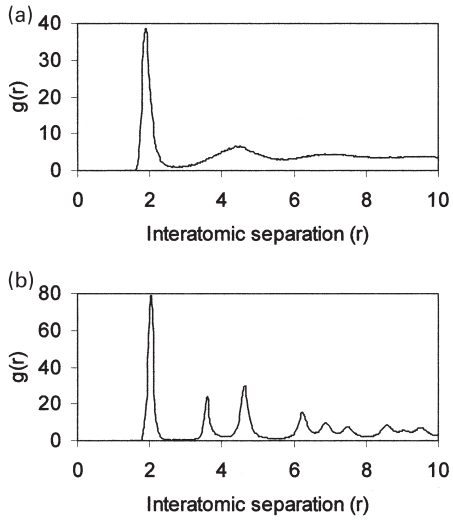

FIGURE 10 Calculated Mg–O RDF after (a) 1 ps of dynamical simulation; (b) at the end of the simulation (final structure).

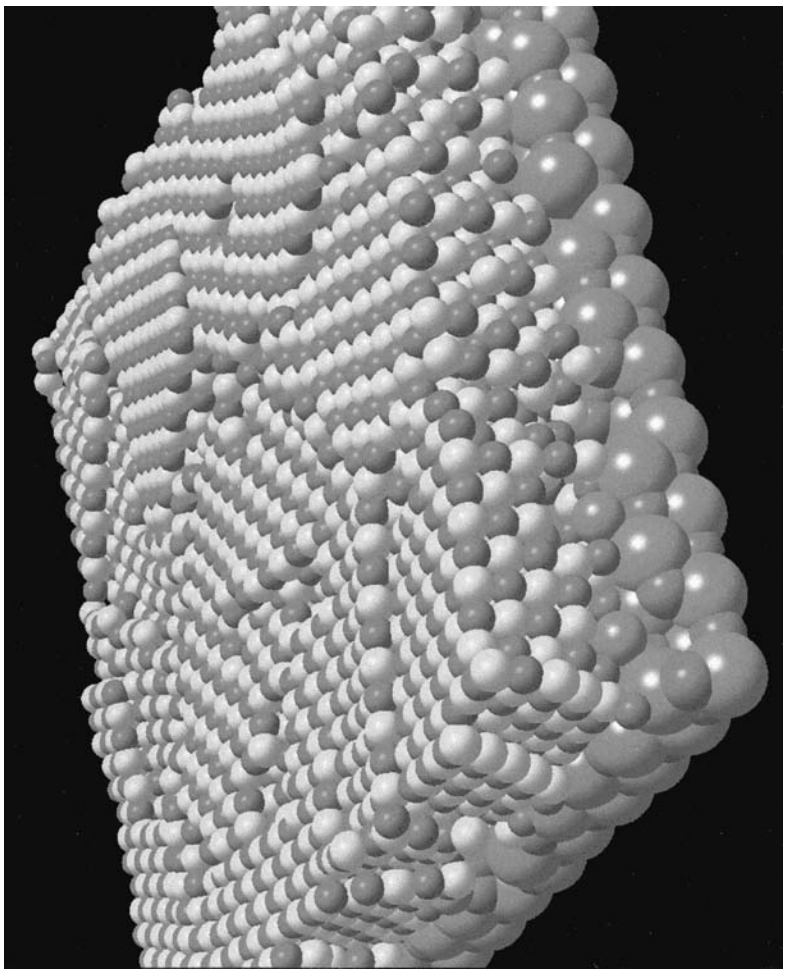

FIGURE 11 Segment (25%) of the MgO/BaO(001) simulation cell. The small dark spheres are oxygen, the small light spheres are magnesium and the large spheres, barium.

The final MgO thin film comprises between 5 and 6 layers and adopts the rocksalt-structure as expected; notice the surface of the MgO thin film is not atomically flat. Mg–O bond distances within the thin film range from 1.8 to 2.3 Å with an average of 2.1 Å suggesting little strain within the film lattice as the natural MgO bond distance is 2.1 Å. In addition, the average Mg–O bond distance for the interfacial MgO plane is 2.0 Å indicating that the interfacial region is strained compared with MgO regions further from the interface. Such an observation is consistent with recent experimental studies on supported oxide thin films, which suggest that the strain within the thin film is not observed beyond the few layers closest to the interface [46].

Defects

At the interfacial region, the MgO and BaO are highly defective and comprise a much lower density of ions compared with the "bulk" material. In particular, numerous voids (up to 200 $Å^2$ in size) exist within the MgO and BaO interfacial planes. In addition, barium ions from the support migrate from the surface to occupy either interstitial positions or magnesium lattice sites within the thin film. The displaced magnesium ions accommodate barium lattice positions within the support.

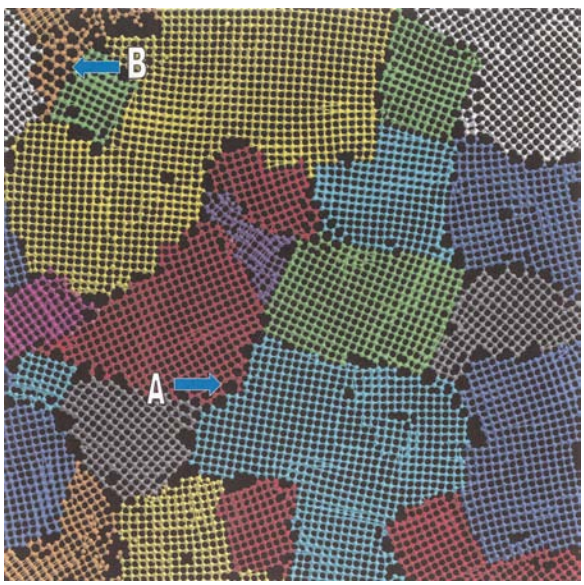

FIGURE 12 Plan view of the full simulation cell (Fig. 11) depicting for reasons of clarity, 2–3 layers of MgO. To aid structural interpretation, the various nano-crystallites are coloured.

Grain-boundaries and Dislocations

A plan view of the MgO thin film is presented in Fig. 12 and shows that the MgO has formed numerous nano-crystallites ranging from 200 to 2000 $Å^2$ in size which are rotated with respect to the underlying BaO surface normal by various angles. The figure demonstrates the wealth of structural features that can be elucidated in such a simulation. These include nano-domains, dislocations, defects, and pseudo-hexagonal MgO, although perhaps most striking are the grain-boundaries that exist where neighbouring nano-crystallites intersect. To aid structural interpretation, graphical techniques were employed to identify, deconvolute and depict the individual features; the elucidation of such three-dimensional atomistic detail is, at present, intractable experimentally.

The atomistic structures of the grain-boundaries within the MgO thin film are similar to those modelled previously in NiO (with good experimental correlation [1]). Since grain-boundaries can be considered as an array of edge-dislocations [48], we have depicted the dislocation core structure of one particular grain-boundary (region "A" in Fig. 12) in Fig. 13. Surprisingly, the core structure is helical, which indicates that the dislocation has screw character in addition to edge character. Mixed screw-edge dislocations are also present within the nano-crystallites in addition to at the domain boundaries.

Another interesting feature concerns the transformation of several MgO regions from a cubic to a pseudo-hexagonal type structure. One extended region (region "B", Fig. 12) is enlarged and presented in Fig. 14. We suggest that the driving force for such a structural transformation is the need to accommodate the lattice misfit; geometrically, a cubic to hexagonal transformation is associated with an increase of about $+30\%$ in the interfacial area. In addition, the hexagonal

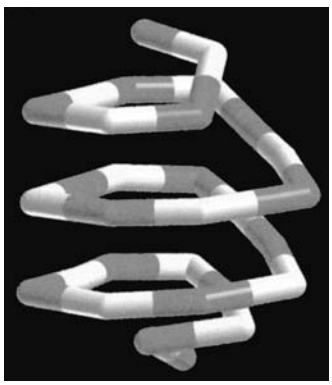

FIGURE 13 Stick representation of the core structure of a screw-edge dislocation, as depicted by region "A" in Fig. 12.

type structure provides considerable structural flexibility with regards to accommodating the lattice misfit. For example a small change in the O–Mg–O bond angles will produce a large change in the interfacial area at low cost energetically [49]. Conversely, for cubic type structures, any compression or expansion along the direction of the bond is energetically expensive and so it is more likely that misfit dislocations will evolve. An analogy can perhaps be drawn between these "pseudo-hexagonal" type structures and a concertina.

The RDF for the final structure is shown in Fig. 10(b) and indicates that the MgO film is crystalline although the RDF peaks are somewhat broader than those of the SrO film demonstrated previously in Fig. 7(e). We attribute the broader RDF peaks of the MgO film to the high concentration of grain-boundaries. In particular, the Mg–O distances within these grain-boundary regions will have a wide distribution around the natural Mg–O bond distance leading to broadening of the peaks.

Epitaxial Relationships

Figure 15 depicts a small region of the MgO and BaO interfacial planes, which shows the epitaxy between the MgO and underlying BaO. For the central region, we see that approximately 12 MgO lattice spacings are matched with 9-lattice spacing for the BaO. Such a commensurate configuration is associated with a +4% lattice misfit. Conversely, for an adjoining region (lower right of the figure), the MgO can be seen to have rotated by about 45° with respect to the underlying BaO with the oxygen of the MgO lying directly above the barium and oxygen

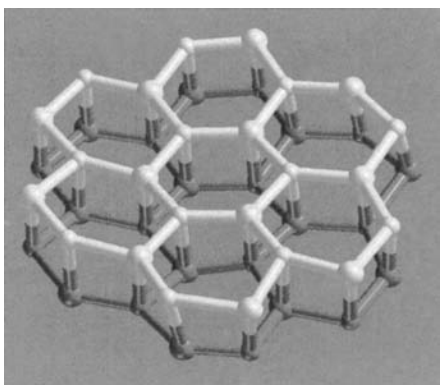

FIGURE 14 Ball and stick representation of an MgO region accommodating a pseudo-hexagonal type structure, as depicted by region "B" in Fig. 12.

lattice positions of the substrate. Here, the "local" lattice misfit is calculated to be +7%. Experimentally, Cotter *et al.* observed a 45° rotation of BaO when supported on MgO [50] (essentially the inverse of the MgO/BaO system considered in this present study). The figure also indicates a reduced density of ions at the interfacial plane.

The driving force enabling the evolution of such configurations is the reduction in the bulk lattice misfit. Clearly, the strain associated with a high lattice misfit is prohibitive and therefore no regions within the MgO/BaO system demonstrate a coherent configuration.

Thus far we have considered rocksalt-structured oxide thin films supported on a rocksalt-structured oxide support. We now explore the structures of a rocksalt-structured oxide supported on a perovskite substrate. In particular, we consider MgO supported on $SrTiO_3$(001). An added complexity of this system is that $SrTiO_3$ can be terminated with either a TiO_2 or an SrO plane and therefore we will

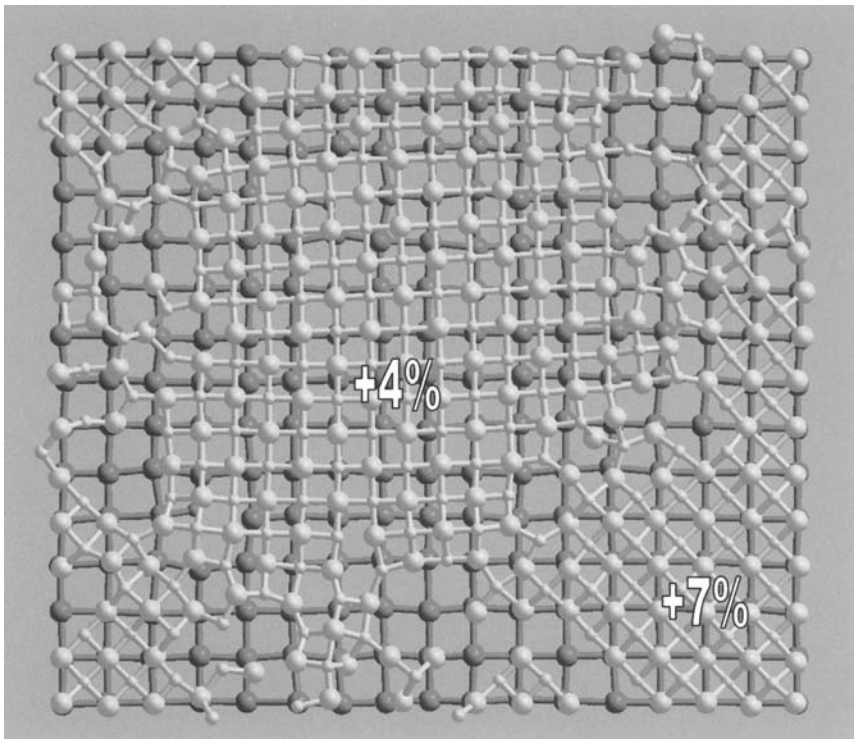

FIGURE 15 Ball and stick representation of a small segment of the MgO and BaO interfacial planes, which shows the epitaxy between the MgO and underlying BaO support.

be able to determine whether the structure and/or the surface termination of the substrate has any influence on the structure of the film it supports.

$MgO/SrTiO_3(001)$

In accordance with the preceding sections, the $MgO/SrTiO_3(001)$ system (+7.4% bulk misfit) was generated using an amorphisation and recrystallisation technique. Further details of the simulation for this particular system can be found elsewhere [51].

SrO Terminated

The interfacial structure for the $MgO/SrTiO_3(001)$ (SrO terminated) is depicted in Fig. 16. For clarity, only a quarter of the full simulation cell is shown. However, the segment presented is of sufficient size to provide an illustration of the main features of the full simulation cell. The supported MgO thin film accommodates the rocksalt type structure and exposes the (001) plane at both the interface and the surface of the thin film. The number of layers within the MgO thin film is between four and five therefore the surface of the MgO thin film is not atomically flat; rather the surface comprises many steps. The average nearest neighbour MgO bond distances within the MgO thin film was derived by calculating the RDF for the thin film and was found to be 2.05 Å. This is in accord with an experimental study by Chern and Cheng [52] who found direct evidence to

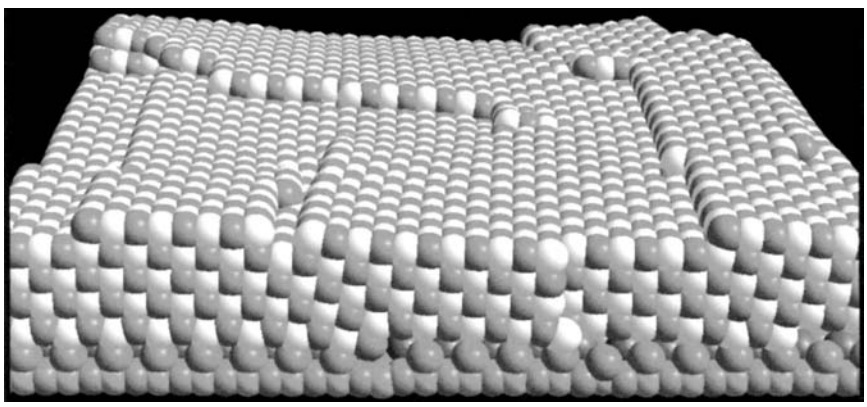

FIGURE 16 Final interfacial configuration for the $MgO/SrTiO_3(001)$ (SrO terminated) system. Slightly less than 25% of the simulation cell is depicted to maintain clarity of the figure. Magnesium ions are represented by the white spheres, oxygen the darker spheres. Only one repeat unit of the underlying $SrTiO_3(001)$ is shown for reasons of clarity.

suggest that the MgO forms with nearly relaxed lattice constant from the first monolayer.

Dislocations

Inspection of the surface of the thin film suggests the presence of dislocations within the supported MgO lattice, which evolve to help accommodate the lattice misfit associated with the system. To aid structural interpretation of the dislocations, the core structure of two neighbouring dislocations have been deconvoluted using graphical techniques and are presented in Fig. 17. The dislocations have both screw and edge components and are similar to those observed previously.

Defects

The interfacial SrO and underlying TiO_2 planes accommodate many isolated oxygen and strontium vacancies including vacancy association. In addition,

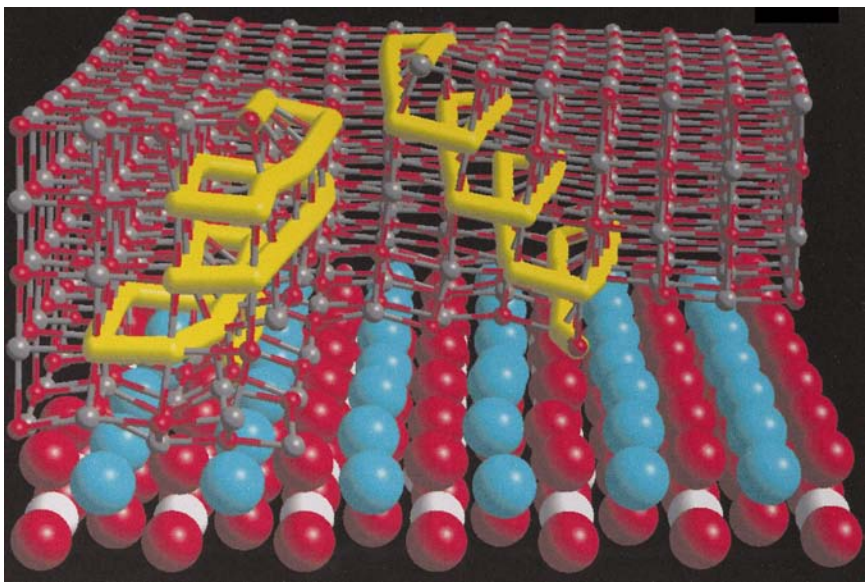

FIGURE 17 Structural representation of two screw-edge dislocations identified within the $MgO/SrTiO_3(001)$ (SrO terminated) system (Fig. 16). The MgO thin film is represented as a ball and stick model with the core structure of the dislocations (stick model) coloured yellow. Much of the MgO has been "cut away" to ensure clarity of the relative positions of the dislocation cores within the MgO lattice. The underlying $SrTiO_3$ is depicted using a sphere model representation. Oxygen is coloured red, magnesium is grey, strontium is blue and titanium, white.

intermixing of cations across the interface is observed: strontium ions migrate to accommodate magnesium lattice positions within the interfacial MgO plane and the displaced magnesium ions accommodate strontium lattice positions within the interfacial SrO plane.

MgO/$SrTiO_3$(001); TiO_2 Terminated

The interfacial structure between an MgO film and a TiO_2 terminated $SrTiO_3$(001) substrate is shown in Fig. 18. Again, for reasons of clarity, only a quarter of the full simulation cell is shown. The supported MgO thin film accommodates the rocksalt type structure and exposes the (001) plane at both the interface and the surface of the thin film. There are four layers within this MgO film; the surface of which is atomically flat (albeit corrugated in certain regions) in contrast to the MgO/$SrTiO_3$(SrO terminated) system. Moreover, the MgO thin film contains no dislocations: We tentatively suggest (surprisingly) that the critical thickness for dislocation evolution for TiO_2 terminated thin films is larger than that SrO terminated systems. In particular, the MgO thin film is able to accommodate the lattice misfit via a remarkable structural transformation.

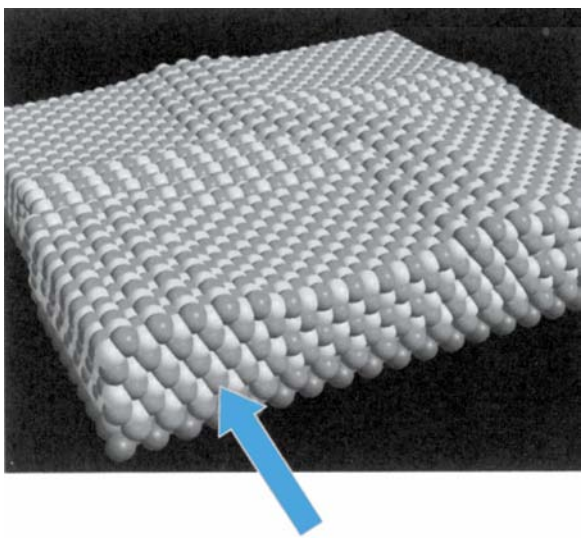

FIGURE 18 Final interfacial configuration for the MgO/$SrTiO_3$(001) (TiO_2) terminated system; (a) sphere representation of just under 25% of the full simulation cell. Magnesium species are represented by the white spheres, oxygen the darker spheres. Only one repeat unit of the underlying $SrTiO_3$(001) is shown for reasons of clarity.

Close inspection of the MgO thin film structure (Fig. 19) reveals regions of the MgO, which accommodate a pseudo-hexagonal type structure forming an interconnecting (90°) network of hexagonal pipes. The network is interdispersed with regions of rocksalt-structured MgO. Similar structures have been observed previously [19]. The bottom right insert of Fig. 19 depicts the surface layer of the MgO thin film illustrating the rumpling of the interfacial MgO plane.

A theoretical study by Recio *et al.* [49] suggests that for small $(Mg_3O_3)_n$ clusters, hexagonal ("tubes") rather than cubic symmetry is energetically favourable for small values of n. As n increases, the energy difference is reduced until the cubic structure becomes energetically favourable. We predict that at greater thin film thicknesses, the pseudo-hexagonal structure of the MgO cannot be sustained and that the thin film will revert to a rocksalt type structure presumably with the evolution of dislocations to help accommodate the lattice misfit.

Thus far, we have amorphised and recrystallised rocksalt-structured oxides. We now extend our study to explore whether the amorphisation and recrystallisation methodology is applicable to fluorite-structured oxides. In particular, we consider CeO_2 supported on ZrO_2, which is associated with a $+7\%$ lattice misfit [53].

$CeO_2/ZrO_2(111)$

Ceria and materials containing ceria are used as catalysts and promoters in several heterogeneous catalytic reactions [54] and comprise a major component

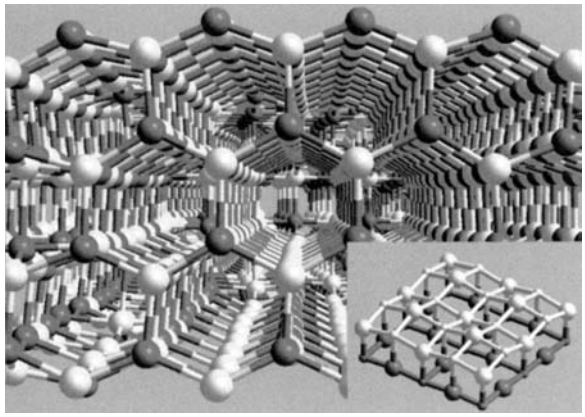

FIGURE 19 Ball and stick representation (with perspective) of a side view looking along the arrow of Fig. 18 of the $MgO/SrTiO_3(001)$ (TiO_2) terminated system depicting only the MgO thin film illustrating the "pseudo-hexagonal" type structure adopted by the supported MgO thin film. Part of the inter-connecting cubic MgO can also be seen when one views through the central hexagonal pipe. To aid structural interpretation, an insert is included, bottom right, which depicts the surface layer of the MgO thin film.

in three-way catalysts (TWC), which are used for the treatment of automobile exhaust gases. The oxygen storage capacity (OSC) of these materials is one of their key properties and arises from the ability of cerium to shift between Ce^{4+} and Ce^{3+}. Accordingly, ceria based catalysts can work in both oxidizing and reducing conditions, converting carbon monoxide, nitrogen oxides and hydrocarbons into non-toxic products. For many CeO_2 based catalytic systems, the CeO_2 is supported on substrates such as Al_2O_3 [55], ZrO_2 [53] and YSZ [56], which enhance the catalytic properties of the material [55]. Clearly, to derive improved materials it is necessary to determine structurally the features that evolve within the CeO_2 when supported and which may be responsible for the remarkable catalytic properties of the material. Accordingly, we employ simulation techniques to address these issues using the $CeO_2/ZrO_2(111)$ as a model system and using a simulated amorphisation and recrystallisation methodology.

To generate the $CeO_2/ZrO_2(111)$ system, a CeO_2 thin film (two repeat units thick) was supported on a $ZrO_2(111)$ substrate using a simulation cell size of about 17,800 $Å^2$ [53]. Amorphisation was induced by constraining the CeO_2 under compression. In particular, we considered two compressions of the CeO_2 thin film (following Eq. (2)): (a) 15%; (b) 31%. The amorphisation and recrystallisation process in both cases was monitored with the RDF and MSD of the ions during the dynamical simulation.

15% Compression

The MSD of cerium and oxygen ions during dynamical simulation is presented in Fig. 20. It can be seen that for cerium, the MSD increases rapidly at the beginning of the simulation, during the amorphisation process, while after 50 ps it reaches a plateau indicating much reduced diffusion as the recrystallisation nears completion. For the oxygen ions, we observe the same behaviour at the

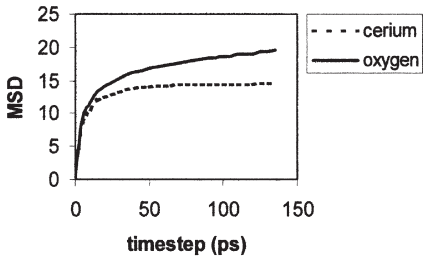

FIGURE 20 Calculated cerium and oxygen MSD within the $CeO_2/ZrO_2(111)$ system during dynamical simulation performed at 2000 K. The units for the MSD are $Å^2$.

beginning of the amorphisation, whilst at the end, the gradient of the curve remains positive indicating that the oxide ions are still highly mobile. The shape of the MSD curves suggests that the thin film does not melt [44].

RDF for Ce–O within the CeO_2 thin film are shown for the initial configuration in Fig. 21(a), then after 0.25 ps in Fig. 21(b), 25 ps in Fig. 21(c) and for the final structure in Fig. 21(d). After 0.25 ps, the CeO_2 thin film loses some long range-order, suggesting an amorphous transition without melting. At 25 ps, the ceria thin film starts to regain long-range order, indicating recrystallisation but the RDF for the final structure depicts broad peaks indicating poor crystallinity. In addition, inspection of the final structure, (Fig. 22), reveals large crystalline regions separated by amorphous regions.

31% Compression

Structural characterisation of the amorphisation and recrystallisation induced via a 31% compression of the CeO_2 thin film is presented in Fig. 23(a)–(c) for the initial structure, after 0.25 ps and final structure respectively. In accord with the 15% compression, the CeO_2 undergoes an amorphous transition, which then recrystallises; the RDF shown in Fig. 23(b) demonstrates almost no long-range order. However, in contrast to the broad peaks observed for the previous final structure following 15% compression (Fig. 21(d)), the RDF here exhibits sharp peaks (Fig. 23(c)). Moreover, the final structure of the supported CeO_2 exhibits no observable amorphous regions. Clearly, for this system the mechanism for inducing amorphisation exacts a critical influence on the final structure. For example, the 15% compression led to a final structure that remained partially amorphous. Conversely, employing an initial 31% compression led to final structures, which demonstrated no amorphous regions; misfits higher than 31% (specifically 50%) resulted in catastrophic failure of the simulation.

We now consider in more details the structural features for the CeO_2/ZrO_2(111) system where amorphisation was induced by imposing an initial 31% compression on the CeO_2 thin film.

Structural Features

Inspection of the final structure of the CeO_2/ZrO_2(111) system, shown in Fig. 23(c), reveals that the thin film has recrystallised completely into the fluorite structure, with the CeO_2 exposing the (111) plane at both the interface and surface layers. The thin film comprises approximately five CeO_2 repeat units with

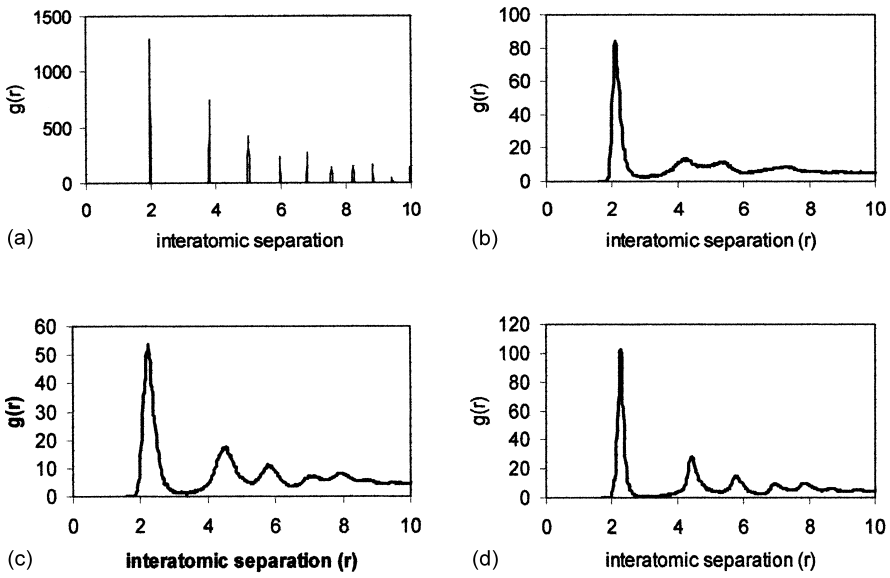

FIGURE 21 Calculated Ce–O RDF within the CeO_2 thin film during dynamical simulation performed at 2000 K: (a) initial; (b) after 0.25 ps; (c) 25 ps and (d) at the end of the simulation. Interatomic separations are in Å.

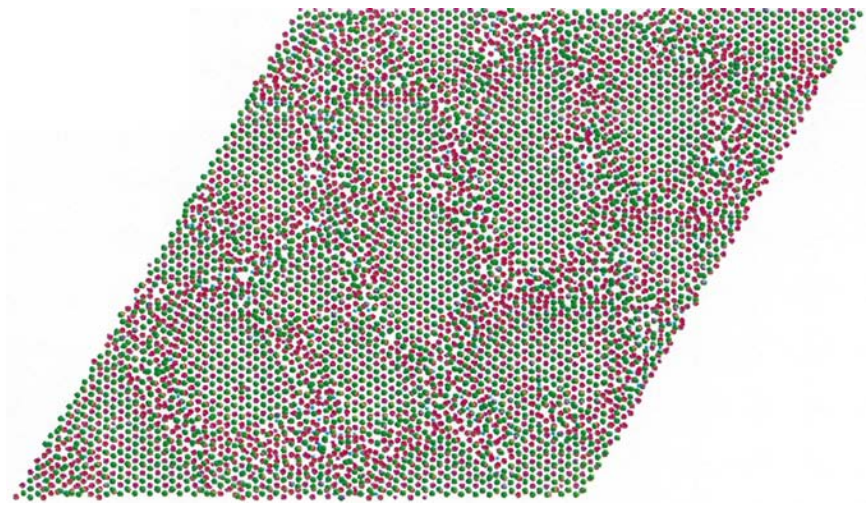

FIGURE 22 Plan view of the $CeO_2/ZrO_2(111)$ system. Only two units of the support are presented for clarity. Zirconium is coloured light blue, cerium is magenta, oxygen (ZrO_2) is red and oxygen (CeO_2) is green.

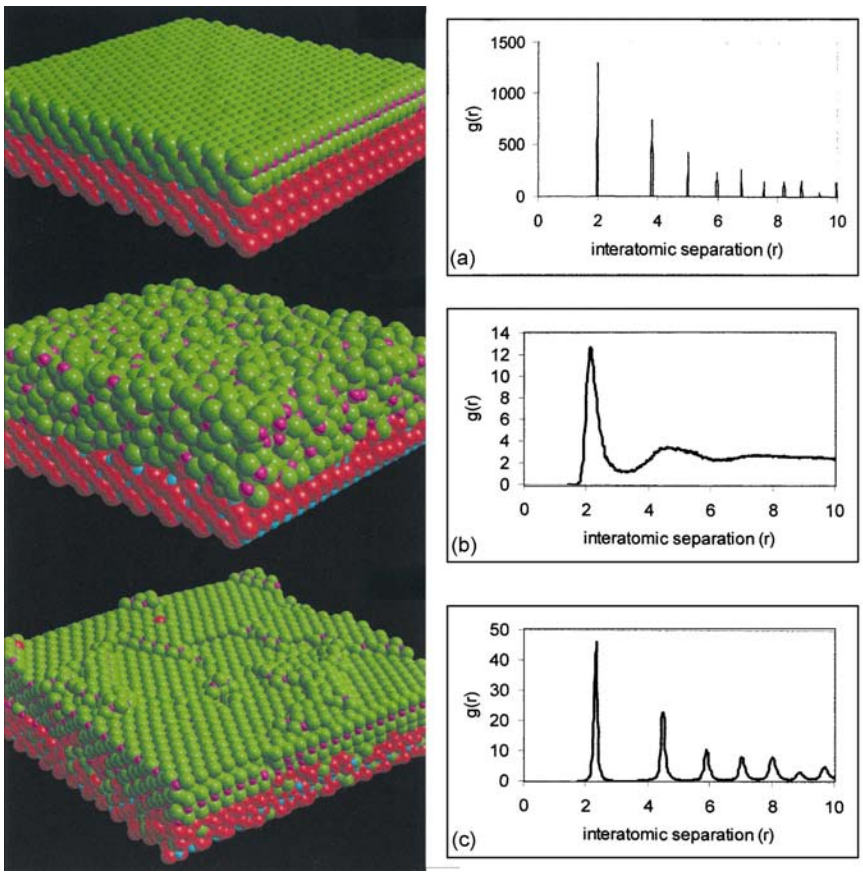

FIGURE 23 Sphere model representations of the $CeO_2/ZrO_2(111)$ interface during dynamical simulation performed at 3400 K: (a) starting structure; (b) after 0.25 ps and (c) final structure. For reason of clarity, only part of the full simulation cell and three planes of the support are depicted. Zirconium is coloured light blue, cerium is magenta, oxygen (ZrO_2) is red and oxygen (CeO_2) is green. To the right of each figure the corresponding Ce–O RDF is presented. Interatomic separations are measured in Å.

an incomplete surface layer of around 25% occupancy, which comprises small clusters ranging from Ce_2O_4 and Ce_4O_8, to larger clusters up to 500 $Å^2$ in size.

Epitaxial Relationships

The CeO_2 thin film lies almost coherent with the underlying ZrO_2 support, with the CeO_2 accommodating a 19×19 $CeO_2(111)/20 \times 20$ $ZrO_2(111)$ pattern with

no rotation of the CeO_2 with respect to the underlying ZrO_2. The lattice misfit associated with such a configuration is therefore reduced from a $+6.7\%$ based upon 20 CeO_2 units lattice matched with 20 ZrO_2 units (bulk misfit) to $+1.6\%$ based upon 19 CeO_2 units lattice matched with 20 ZrO_2 units (final structure). To maintain such a configuration, the CeO_2 lattice must be compressed by 1.6% to accommodate the misfit, which corresponds theoretically to a "lattice parameter" of 5.34 Å. Experimentally, Dmowski *et al.*, who explored the structure and oxygen storage properties of 20 Å CeO_2 films on zirconia [57] found the CeO_2 lattice parameter to be reduced from 5.41 to 5.38 Å. In addition, they observed no rotation of the CeO_2 with respect to the underlying support in accord with our findings.

Defects

A detailed analysis of the system using molecular graphic techniques revealed that the system comprises cerium (0.8%) and zirconium (0.3%) vacancies that are charge compensated by associated oxygen vacancies. Analysis of the interfacial

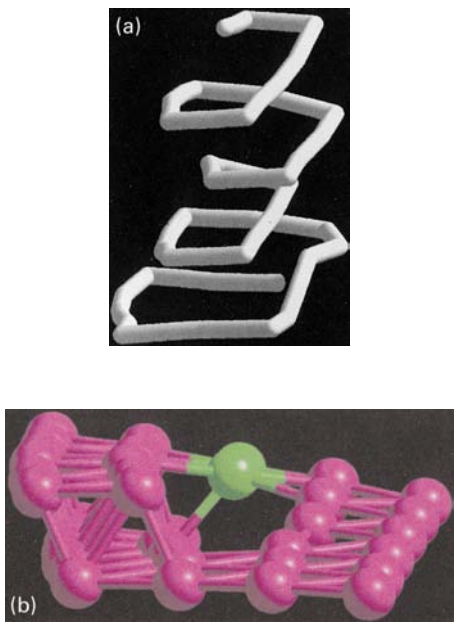

FIGURE 24 Stick model representation of a screw-edge dislocation (core structure) within the supported CeO_2 thin film; (a) stick model representation depicting the spiral of cerium ions; (b) ball and stick model representation illustrating more clearly the edge component (light green spheres).

layers indicates interdiffusion between zirconia and ceria ions across the interfacial plane.

Dislocations

Careful inspection of the structure revealed dislocation networks including pure edge and mixed screw-edge, which have evolved within the system. The latter, as shown in Fig. 24(a), traverses the entire thickness of the CeO_2 thin film and moreover, extends into the first layer of the ZrO_2 support, resulting in considerable perturbation of the underlying ZrO_2 support. In response, zirconium and oxygen ions migrate from the support to form a large associated defect cluster, about 300 $Å^2$ in size, which emanates from the base of the dislocation core. Figure 24(b) depicts more clearly the edge component of this screw-edge dislocation. We also observe pure edge dislocations within both the CeO_2 thin film and the ZrO_2 support (Fig. 25). Misfit edge-dislocations, uniformly distributed, were also identified upon viewing cross-sections of the interface (Fig. 26). Such uniformly distributed misfit edge-dislocations, in planes parallel with the interface or across the interface, have been observed, using transmission electron microscopy, in semiconductor systems [7].

CONCLUSION

In this study, we have demonstrated that the application of three simulation methodologies: "atom deposition", "layer-by-layer" and "amorphisation and recrystallisation" enables one to explore the growth, nucleation and structure of various thin-film, oxide–oxide interface systems. Moreover, the computer-

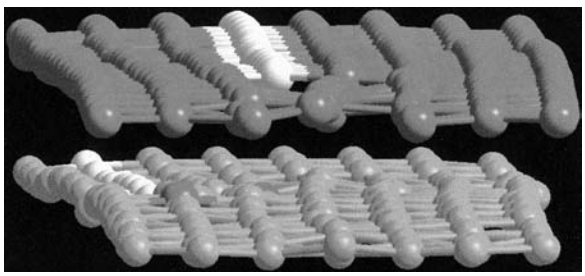

FIGURE 25 Ball and stick representation of two edge dislocations (white spheres) within the interfacial ZrO_2 layer (bottom) and second interfacial CeO_2 layer (top). The remaining planes have been omitted to preserve clarity. Zirconium is coloured light grey and cerium dark grey.

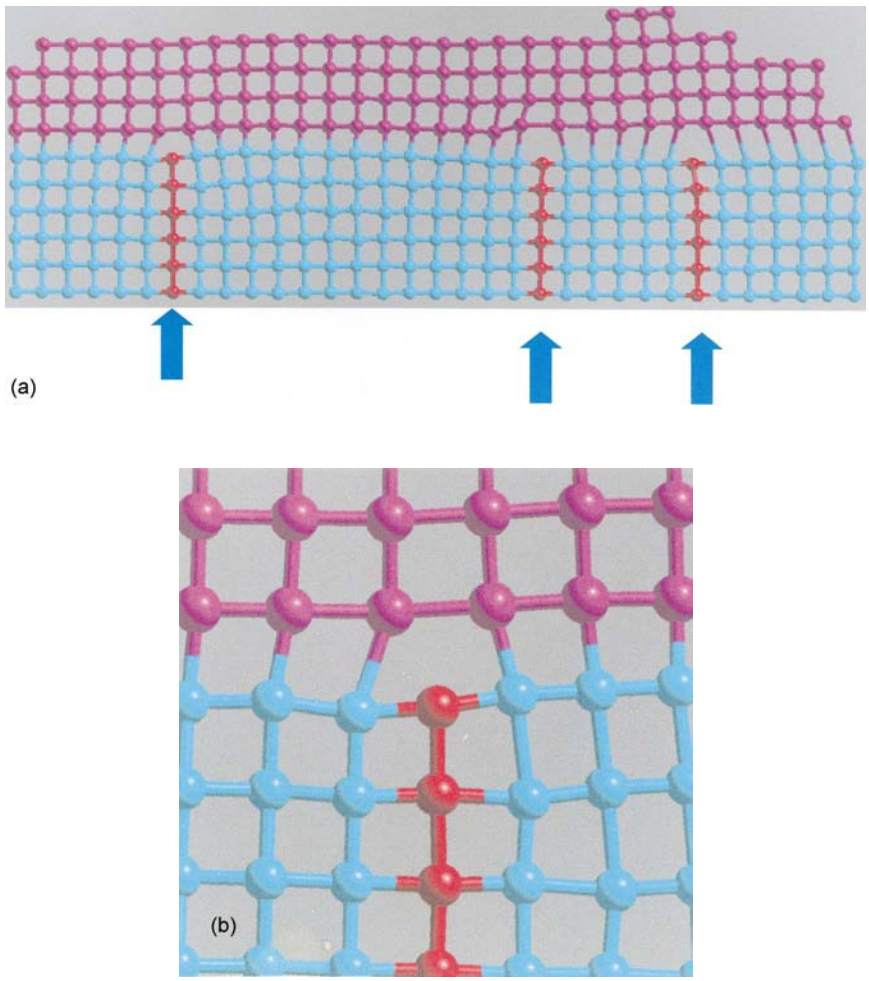

FIGURE 26 (a) Ball and stick representation of a cross-section of the $CeO_2(111)/ZrO_2(111)$ interface depicting the regular array of dislocations (red); (b) enlarged segment depicting more clearly, the core structure. For reasons of clarity only the cation sublattice is shown. Cerium ions are magenta and zirconium ions are light blue.

generated models reproduce many of the complex phenomena observed experimentally within thin films supported on lattice-mismatched substrates. The phenomena exhibited within the models include epitaxial relationships, such as the orientation of the thin film with respect to the underlying support and the commensurate relationships that exist at the interfacial region. The models also demonstrate the evolution of various structural modifications within both the thin film and the underlying support. Of these modifications, dislocation networks of

both edge and mixed screw-edge character are identifiable as is the critical thickness beyond which they are initiated. Defects, in the forms of vacancies, interstitials and substitutionals (along with complex defect cluster configurations) are also observable. The models demonstrate reduced interfacial ion densities and the intermixing of ions across the interfacial plane, and clearly show rotations of nano-crystallites comprising the thin film and the intersections which give rise to complex grain-boundary networks (MgO/BaO(001)). Since the positions of all the atoms within the system are defined explicitly, detail at the atomistic level of each of the structural features can be presented using graphical techniques with full three-dimensional atomistic clarity. Simulation thus provides a powerful tool with which to complement experimental studies.

It is a particularly important theme, within the simulation approaches considered here, that the systems were allowed to evolve naturally in response to the lattice misfit and interactions across the interface. Consequently, the starting configuration does not influence (artificially) the final structures. In addition, for the amorphisation and recrystallisation procedure, large simulation cell sizes were considered enabling the synergy of interaction between neighbouring structural features to be implicit within the simulation. The models derived are likely therefore to reflect real systems.

The considerable structural modifications associated with supporting a thin film will lead to changes in the material properties. For example, for the CeO_2/ZrO_2 system, the reduced coordinative saturation of ions at the surface of the CeO_2 thin film will influence ionic lability; weakly bound oxygen ions are more likely to participate in oxidation catalysis. The understanding of factors, which result in labile surface ions such as defects, dislocations and grain-boundaries (all of which we have "observed" in this present study) will have important implications for the catalytic properties of the material. The understanding of how such configurations arise and moreover how they can be controlled or optimised is an important issue in the design of improved catalytic systems.

An additional consideration for CeO_2 based catalysts is the mobility of oxygen within the CeO_2 lattice, which is linked with the oxygen storage capacity of the material. The models generated in this present study are ideal starting points with which to explore oxygen mobility. Specifically, the dislocation, grain-boundary and defect structure of the supported material is likely to influence considerably the oxygen mobility. Accordingly, such a study will be the focus of future work.

Models of catalytic systems generated using the methodology presented here will also be useful starting points for computationally more expensive quantum mechanical calculations, which will enable one to probe the reactivity and potential reaction mechanisms of the material. Clearly, constructing the trial or

starting structure using atomistic simulation affords a much faster route for generating realistic structures compared with a wholly quantum mechanical approach.

One important issue is to determine how nucleation and growth mechanisms direct the structure of the supported thin film. For example, the amorphisation and recrystallisation methodology enables low energy configurations to be determined. Conversely, the structures determined using atom deposition and layer-by-layer will reflect the (perhaps considerable) structural influences of growth and nucleation. Here, the final configurations are likely to exist in metastable states, which are of higher energy than those generated using amorphisation and recrystallisation. To appreciate fully the potential differences, and hence determine the influence of growth and nucleation on the structure, the atom deposition methodology must be employed with simulation cell sizes commensurate to those of the amorphisation and recrystallisation. For such a study, we must await increased computational resources.

References

[1] Sutton, A.P. and Balluffi, R.W. (1995) Interfaces in Crystalline Materials, Monographs on the Physics and Chemistry of Materials (Oxford University press, Oxford) **Vol. 51**.

[2] Chambers, S.A. (2000) "Epitaxial growth and properties of thin film oxides", *Surf. Sci. Rep.* **39**, 105.

[3] Koster, A.J., Ziese, U., Verkleij, A.J., Janssen, A.H. and de Jong, K.P. (2000) "Three-dimensional transmission electron microscopy: a novel imaging and characterization technique with nanometer scale resolution for materials science", *J. Phys. Chem.* **104**, 9368.

[4] Stampe, P.A. and Kennedy, R.J. (1998) "X-Ray characterization of MgO thin films grown by laser ablation on $SrTiO_3$ and $LaAlO_3$", *J. Cryst. Growth* **191**, 478.

[5] Zandbergen, H.W., Connolly, E., Graboy, I.E., Svetchnikov, V.L. and Kaul, A.R. (2000) "HREM characterisation of interfaces in $YBa_2Cu_3O_7$-delta/CeO_2/R-Al_2O_3 structures", *Physica C* **329**, 37.

[6] Patriarche, G., Meriadec, C., LeRoux, G., Deparis, C., Sagnes, I., Harmand, J.-C. and Glas, F. (2000) "GaAs/GaAs twist-bonding for compliant substrates: interface structure and epitaxial growth", *Appl. Surf. Sci.* **164**, 15.

[7] Rocher, A. and Snoeck, E. (1999) "Misfit dislocations in (001) semiconductor heterostructures grown by epitaxy", *Mater. Sci. Engng. B* **67**, 62.

[8] Gorbenko, O.Yu., Graboy, I.E., Kaul, A.R. and Zandbergen, H.W. (2000) "HREM and XRD characterization of epitaxial perovskite manganites", *J. Magn. Magn. Mater.* **211**, 97.

[9] McKee, R.A., Walker, F.J. and Chisholm, M.F. (1998) "Crystalline oxides on silicon: the first five monolayers", *Phys. Rev. Lett.* **81**, 3014.

[10] Ernst, F., Recnik, A., Langjahr, P.A., Nellist, P.D. and Ruhle, M. (1999) "Atomistic structure of misfit dislocations in $SrZrO_3$/$SrTiO_3$ interfaces", *Acta Mater.* **47**, 183.

[11] Stoneham, A.M., Ramos, M.M.D. and Sutton, A.P. (1993) "How do they stick together? The statics and dynamics of interfaces", *Phil. Mag. A* **67**, 797.

[12] Kubo, M., Oumi, Y., Miura, R., Stirling, A., Miyamoto, A., Kawasaki, M., Yoshimoto, M. and Koinuma, H. (1997) "Atomic control of layer-by-layer epitaxial growth on $SrTiO_3$(001): MD simulations", *Phys. Rev. B* **56**, 13535.

[13] Sayle, D.C. (1999) "Strain reduction in supported materials; the formation of cracks and dislocations", *J. Mater. Chem.* **9**, 607.

[14] Shluger, A.L., Rohl, A.L. and Gay, D.H. (1995) "Properties of small clusters at ionic surfaces: Properties of $(NaCl)_n$ clusters $n = 1-48$ at the (001) MgO surface", *Phys. Rev. B* **51**, 13631.
[15] Novaco, A.D. and McTague, J.P. (1977) "Orientational epitaxy—the orientational ordering of incommensurate structures", *Phys. Rev. Lett.* **38**, 1286.
[16] Tasker, P.W. and Stoneham, A.M. (1987) "The stabilisation of oxide and oxide-metal interfaces by defects and impurities", *Journal de Chemie Physique* **84**, 149.
[17] Balluffi, R.W., Brokman, A. and King, A.H. (1982) "CSL DSC lattice model for general crystal–crystal boundaries and their line defects", *Acta metall.* **30**, 1453.
[18] Sayle, T.X.T., Catlow, C.R.A., Sayle, D.C., Parker, S.C. and Harding, J.H. (1993) "Computer simulation of thin film heteroepitaxial ceramic interfaces using a near-coincidence-site lattice theory", *Phil. Mag. A* **68**, 565.
[19] Sayle, D.C., Maicaneanu, S.A., Slater, B. and Catlow, C.R.A. (1999) "Exercising control over the influence of the lattice misfit on the structure of oxide–oxide thin film interfaces", *J. Mater. Chem.* **9**, 2779.
[20] Wolf, D. and Jaszczak, J.A. (1993) "Tailored elastic behaviour of multilayers through controlled interface structure", *J. Comput.-Aid. Mater. Des.* **1**, 111.
[21] Zhou, S.J., Beazley, D.M., Lomdahl, P.S. and Holian, B.H. (1997) "Large-scale molecular dynamics simulations of three-dimensional ductile failure", *Phys. Rev. Lett.* **78**, 479.
[22] Sepliarsky, M., Phillpot, S.R., Wolf, D., Stachiotti, M.G. and Migoni, R.L. (2000) "Atomic-level simulation of ferroelectricity in perovskite solid solutions", *Appl. Phys. Lett.* **76**, 3986.
[23] Valladares, A., White, J.A. and Sutton, A.P. (1998) "First principle simulations of the structure, formation, and migration energies of kinks on the 90° partial dislocation in silicon", *Phys. Rev. Lett.* **81**, 4903.
[24] Duffy, D.M. (1986) "Grain boundaries in ionic crystals", *J. Phys. C: solid State Phys.* **19**, 4393.
[25] Watson, G.W., Kelsey, E.T., de Leeuw, N.H., Harris, D.J. and Parker, S.C. (1996) "Atomistic simulation of dislocations, surfaces and interfaces in MgO", *J. Chem. Soc., Faraday Trans.* **92**, 433.
[26] Watson, G.W., Kelsey, E.T. and Parker, S.C. (1999) "Atomistic simulation of screw dislocations in rock salt structured materials", *Phil. Mag. A* **79**, 527.
[27] Sayle, D.C. (1999) "The predicted 3-D atomistic structure of an interfacial screw-edge dislocation", *J. Mater. Chem.* **9**, 2961.
[28] Sayle, D.C. and Watson, G.W. (2000) "Simulated amorphisation and recrystallisation: nanocrystallites within meso-scale supported oxides", *J. Mater. Chem.* **10**, 2241.
[29] Serra, A., Bacon, D.J. and Pond, R.C. (1999) "Dislocations in interfaces in the hcp metals—I. Defects formed by absorption of crystal dislocations", *Acta. Mater.* **47**, 1425.
[30] Levay, A., Mobus, G., Vitek, V., Ruhle, M. and Tichy, G. (1999) "Structure of misfit dislocations in niobium–saphire interfaces and strength of interfacial bonding: an atomistic study", *Acta Mater.* **47**, 4143.
[31] Oyama, N., Ohta, E., Takeda, K., Shiraishi, K. and Yamaguchi, H. (1999) "First-principles calculation for misfit dislocations in InAs/GaAs(110) heteroepitaxy", *Surf. Sci.* **433**, 900.
[32] Phillpot, S.R., Keblinski, P., Wolf, D. and Cleri, F. (1999) "Synthesis and characterization of a polycrystalline ionic thin film by large-scale molecular dynamics simulation", *Interface Sci.* **7**, 15.
[33] Wunderlich, W., Fujimoto, M. and Ohsato, H. (2000) "Molecular dynamics calculations about misfit dislocations at the $TiO_3/SrTiO_3$ interface", *Thin Solid Films* **375**, 9.
[34] Baker, J. and Lindgard, P.-A. (1999) "Heteroepitaxial strain in alkali halide thin films: KCl on NaCl", *Phys. Rev. B* **60**, 16941.
[35] Dong, L., Schnitker, J., Smith, R.W. and Srolovitz, D.J. (1998) "Stess relaxation and misfit dislocation nucleation in the growth of misfiting films: a molecular dynamics study", *J. Appl. Phys.* **83**, 217.
[36] Sayle, D.C., Catlow, C.R.A., Perrin, M.-A. and Nortier, P. (1996) "Computer modelling of the V_2O_5/TiO_2 interface", *J. Phys. Chem.* **100**, 8940.
[37] Sayle, D.C., Sayle, T.X.T., Parker, S.C., Harding, J.H. and Catlow, C.R.A. (1995) "The stability of defects in the ceramic interfaces, MgO/MgO and CeO_2/Al_2O_3", *Surf. Sci.* **334**, 170.
[38] Sutton, A.P. and Balluffi, R.W. (1987) "On geometric criteria for low interfacial energy", *Acta metal.* **35**, 2177.

[39] Putna, E.S., Vohs, J.M. and Gorte, R.J. (1996) "Evidence for weakly bound oxygen on ceria films", *J. Phys. Chem.* **100**, 17862.
[40] Bond, G.C., Flamerz, S. and Shukri, R. (1989) "Structure and reactivity of transition-metal oxide monolayers", *Faraday Discuss., Chem. Soc.* **87**, 65.
[41] Gay, D.H. and Rohl, A.L. (1995) "MARVIN: A new computer code for studying surfaces and interfaces and its application to calculating the crystal morphologies of corundum and zircon", *J. Chem. Soc., Faraday Trans.* **91**, 925.
[42] Lewis, G.V. and Catlow, C.R.A. (1985) "Potential models for ionic oxides", *J. Phys. C: Solid State Phys.* **18**, 1149.
[43] Dwivedi, A. and Cormack, A.N. (1990) "A computer simulation study of the defect structure of calcia-stabilized zirconia", *Philos. Mag. A* **61**, 1.
[44] Sayle, D.C. and Watson, G.W. (2001) "Structural exploration of thin film oxide interfaces via simulated amorphisation and recrystallisation", *Surf. Sci.* **473**, 97.
[45] Sayle, D.C., Catlow, C.R.A., Harding, J.H., Healy, M.J.F., Maicaneanu, S.A., Parker, S.C., Slater, B. and Watson, G.W. (2000) "Atomistic simulation methodologies for modelling the nucleation, growth and structure of interfaces", *J. Mater. Chem.* **10**, 1315.
[46] Chern, G. (1997) "Incommensurate growth and interface stability in $MgO/SrTiO_3(001)$", *Surf. Sci.* **387**, 183.
[47] Lind, D.M., Berry, S.D., Chern, G., Mathias, H. and Testardi, L.R. (1992) "Growth and structural characterization of Fe_3O_4 and NiO thin films and superlattices grown by oxygen-plasma-assisted molecular-beam epitaxy", *Phys. Rev. B* **45**, 1838.
[48] Kamien, R.D. and Lubensky, T.C. (1999) "Minimal surfaces, screw dislocations, and twist grain boundaries, Phys", *Rev. Lett.* **82**, 2892.
[49] Recio, J.M., Pandey, R., Ayuela, A. and Kunz, A.B. (1993) "Molecular-orbital calculations on $(MgO)_n$ and $(MgO)_{n+}$ clusters $n = 1-13$;", *J. Chem. Phys.* **98**, 4783.
[50] Cotter, M., Campbell, S., Egdell, R.G. and Mackrodt, W.C. (1988) "Growth of ordered BaO overlayers on MgO(001)", *Surf. Sci.* **197**, 208.
[51] Sayle, D.C. and Watson, G.W. (2001) "The atomistic structures of $MgO/SrTiO_3(001)$ and $BaO/SrTiO_3(001)$ using simulated amorphization and recrystallization", *J. Phys. Chem.* **105**, 5506.
[52] Chern, G. and Cheng, C. (1999) "Interface matching in oxides of rocksalt/rocksalt(001) and rocksalt/perovskite(001)", *J. Vac. Sci. Technol. A* **17**, 1097.
[53] Maicaneanu, S.A., Sayle, D.C. and Watson, G.W. (2001) "Evolution and atomistic structure of dislocations defects and clusters within CeO_2 supported on ZrO_2", *Chem. Commun.*, 289.
[54] Trovarelli, A. (1996) "Catalytic properties of ceria and CeO_2-containing materials", *Catal. Rev. Sci. Eng.* **38**, 439.
[55] Putna, E.S., Bunluesin, T., Fan, X.L., Gorte, R.J., Vosh, J.M., Lakis, R.E. and Egami, T. (1999) "Ceria films on zirconia substrates: models for understanding oxygen-storage properties", *Catal. Today* **50**, 343.
[56] Putna, E.S., Vohs, J.M. and Gorte, R.J. (1997) "Characterization of ceria films on α-$Al_2O_3(0001)$ and polycrystalline zirconia using O_2 TPD with labelled $^{18}O_2$", *Catal. Lett.* **45**, 143.
[57] Dmowski, W., Mamontov, E., Egami, T., Putna, E.S. and Gorte, R. (1998) "Energy-dispersive surface X-ray scattering study of thin ceria overlayer on zirconia: Structural evolution with temperature", *Physica B* **248**, 95.